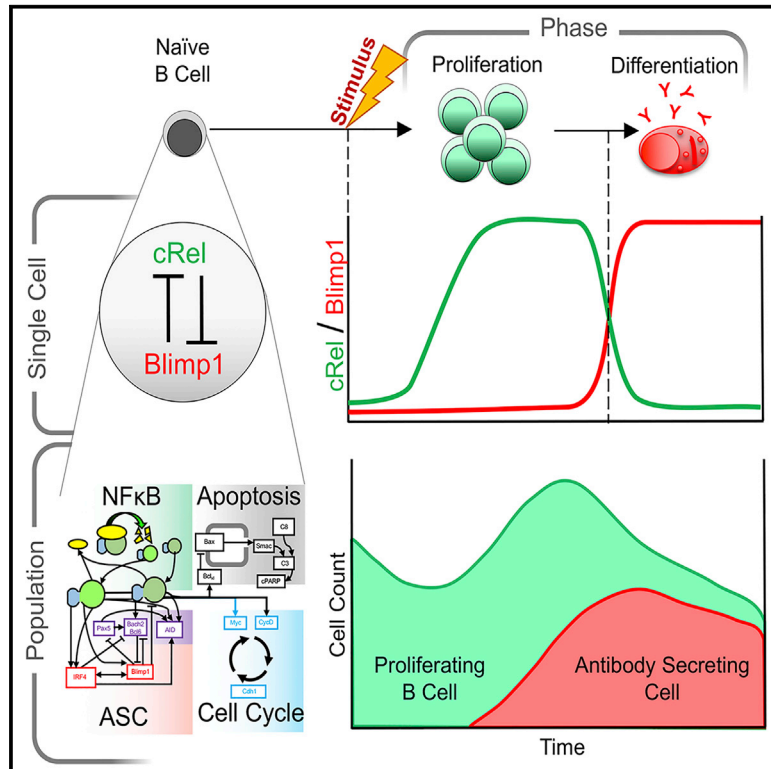# A Regulatory Circuit Controlling the Dynamics of NFκB cRel Transitions B Cells from Proliferation to Plasma Cell Differentiation

## Graphical Abstract



## Authors

Koushik Roy, Simon Mitchell, Yi Liu, ..., Marie Oliver Metzig, Stephen L. Nutt, Alexander Hoffmann

## Correspondence

ahoffmann@ucla.edu

## In Brief

Antibody production requires proper phasing of B cell proliferation and differentiation. Using an iterative systems biology approach, Roy et al. reveal that, although NFκB cRel enables proliferation, it must be downregulated during differentiation. Multi-scale modeling shows how coordinated cRel and RelA dynamics control B cell populations in health and disease.

## Highlights

- cRel drives B cell proliferation but blocks antibody-secreting cell differentiation

- In ASCs, RelA-induced Blimp1 represses cRel via binding the *Rel* enhancer

- NFκB dynamics transition cells across the bi-stable ABC-ASC differentiation network

- Multi-scale model of single-cell-fate decisions explains B cell population dynamics

# A Regulatory Circuit Controlling the Dynamics of NFκB cRel Transitions B Cells from Proliferation to Plasma Cell Differentiation

Koushik Roy,[1,4] Simon Mitchell,[1,4] Yi Liu,[1] Sho Ohta,[1] Yu-sheng Lin,[1] Marie Oliver Metzig,[1] Stephen L. Nutt,[2,3] and Alexander Hoffmann[1,5,*]

[1]Signaling Systems Laboratory, Institute for Quantitative and Computational Biosciences and Department of Microbiology, Immunology, and Molecular Genetics, University of California, Los Angeles, Los Angeles, CA 90095, USA
[2]Walter and Eliza Hall Institute of Medical Research, 1G Royal Parade, Parkville, VIC 3050, Australia
[3]Department of Medical Biology, University of Melbourne, Parkville, VIC 3010, Australia
[4]These authors contributed equally
[5]Lead Contact
*Correspondence: ahoffmann@ucla.edu
https://doi.org/10.1016/j.immuni.2019.02.004

## SUMMARY

Humoral immunity depends on efficient activation of B cells and their subsequent differentiation into antibody-secreting cells (ASCs). The transcription factor NFκB cRel is critical for B cell proliferation, but incorporating its known regulatory interactions into a mathematical model of the ASC differentiation circuit prevented ASC generation in simulations. Indeed, experimental ectopic cRel expression blocked ASC differentiation by inhibiting the transcription factor Blimp1, and in wild-type (WT) cells cRel was dynamically repressed during ASC differentiation by Blimp1 binding the *Rel* locus. Including this bi-stable circuit of mutual cRel-Blimp1 antagonism into a multi-scale model revealed that dynamic repression of cRel controls the switch from B cell proliferation to ASC generation phases and hence the respective cell population dynamics. Our studies provide a mechanistic explanation of how dysregulation of this bi-stable circuit might result in pathologic B cell population phenotypes and thus offer new avenues for diagnostic stratification and treatment.

## INTRODUCTION

The production of antibodies is key for an effective immune response and efficacy of vaccination. Recognition of foreign antigens leads to profound changes within secondary lymphoid organs, including the formation of the germinal center (GC) and extrafollicular foci that allow for the rapid expansion of antigen-specific B cell clones to produce neutralizing antibodies and memory B cells. Indeed, T-cell-independent (TI) and T-cell-dependent (TD) stimulation of B cells generates rapidly proliferating cells known as activated B cells (ABCs). ABCs can differentiate into actively cycling short-lived plasmablasts (PBs), which develop in the early phases of an immune response, and quies-

cent long-lived plasma cells (PCs), which reside in a specialized bone marrow niche. Given that both PBs and PCs are capable of producing antibodies, they are referred to as antibody-secreting cells (ASCs) (Shapiro-Shelef and Calame, 2005). The transition of ABCs to ASCs is coordinated by changes in signaling, gene expression, and chromatin regulatory networks. ABC-specific transcription factors (such as Pax5 and Bach2) and ASC-specific transcription factors (such as Blimp1) regulate distinct genetic programs (Kallies et al., 2007; Nutt et al., 2015). Misregulation of these mutually inhibiting transcription factors, caused by common mutations, can result in B cell lymphomas with poor prognosis (Mandelbaum et al., 2010; Nutt et al., 2015; Xia et al., 2017). Transcription factor NFκB is also dysregulated in many B cell lymphomas (Shaffer et al., 2002b), and its inhibition is lethal to these transformed cells (Ceribelli et al., 2014; Staudt, 2010).

NFκB is a key inflammatory and immune transcription factor consisting of a dozen dimers made up of three activation domain-containing proteins (cRel, RelA, and RelB) and two dimerization partners (p50 and p52) (Hoffmann and Baltimore 2006). In ABCs, the NFκB dimers RelA:p50 and cRel:p50 are induced (Kaileh and Sen, 2012). Whereas cRel activity is required for cell survival, growth, and division during B cell activation (Pohl et al., 2002; Shokhirev et al., 2015), RelA is required for the generation of GC-derived PCs by contributing to Blimp1 activation (Heise et al., 2014). Thus, both cRel and RelA are indispensable for humoral immunity but for different functional reasons. However, a recent study showed that in the genetic disease B cell expansion with NFκB and T cell anergy (BENTA), constitutively active NFκB results in reduced ASC generation (Arjunaraja et al., 2017), suggesting that precise regulation of each NFκB dimer is required for healthy ASC generation.

Mathematical modeling approaches have proven valuable to understanding complex dynamic molecular regulatory networks. ABC population expansion dynamics are well accounted for by a multi-scale model of the intracellular molecular network of NFκB regulating apoptosis and the cell cycle (Mitchell et al., 2018; Shokhirev et al., 2015), and this model proved useful in understanding the function of cRel in cell survival, growth, and division (Shokhirev et al., 2015). In the case of the ASC differentiation circuit, the scarcity of quantitative biochemical data first prompted
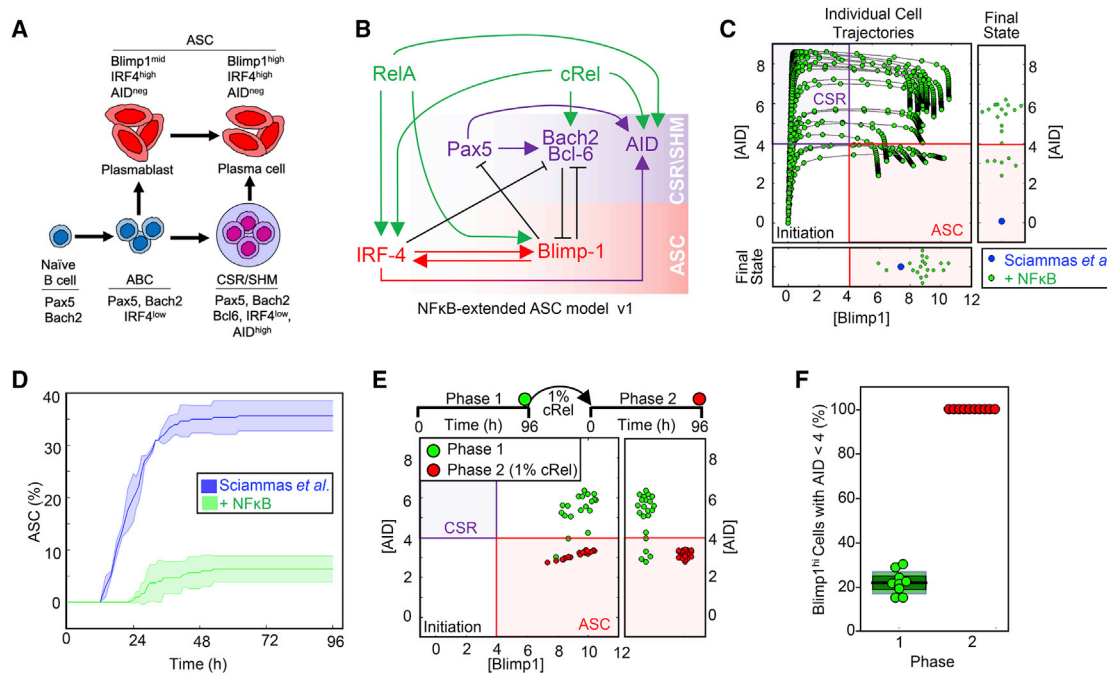
**Figure 1. Mathematical Modeling Predicts that cRel Prevents ASC Differentiation**

(A) Schematic of ASC generation. Stimulation of naive B cells produces ABCs. ABCs either become plasmablasts or undergo CSR and SHM before differentiating into plasma cells. Here, plasmablasts and plasma cells are defined as antibody-secreting cells (ASCs). The regulators and genetic signature that characterize each cell type are indicated.

(B) Schematic of NFκB-extended ASC differentiation model v1. This model was based on a previously published model from Sciammas et al. (2011), to which RelA and cRel were added. RelA- and cRel-mediated regulation is indicated in green, genes associated with the CSR-SHM state are shown in violet, and genes associated with the ASC state are shown in red. Arrows denote activation, and barred lines denote repression.

(C) The trajectories of Blimp1 and AID expression kinetics in the subset of cells that expressed high Blimp1 from a simulation of 125 cells. Four states are defined by two coordinate axes, namely Blimp1$^{low}$AID$^{low}$ (initiation), Blimp1$^{low}$AID$^{high}$ (CSR/SHM), Blimp1$^{high}$AID$^{hi}$, and Blimp1$^{high}$AID$^{low}$ (ASC). The final states are in the rectangular boxes below and on the right, indicating Blimp1 and AID expression, respectively. Green points show the trajectories and final states of the NFκB-extended ASC differentiation model v1. Blue points indicate the final state obtained by all cells in simulations using a previously published model (Sciammas et al., 2011).

(D) Kinetics of ASC differentiation predicted by Sciammas et al. (2011). Shown are the ASC differentiation model and the NFκB-extended ASC differentiation model v1. The percentage of ASCs is plotted with time (h). The solid line indicates the mean, and the shaded region indicates the standard deviation of 3 simulations of 125 cells.

(E) The final states (96 h) reached by cells expressing high Blimp1 in simulations of 125 starting cells with the NFκB-extended ASC differentiation model v1 (phase 1, green) and a subsequent simulation in which cRel activity in those cells was reduced to 1% and trajectories were simulated for 96 h (phase 2, red).

(F) Bar graph of the fraction of ABCs becoming ASCs when cRel was allowed to remain at 100% of its expression (phase 1, green) or when it was forcibly reduced to 1% of its peak (phase 2, red). Median (black), standard deviation (SD; dark green), and standard error of the mean (SEM; light green) are indicated.

logical models that can qualitatively recapitulate the state of regulatory networks in the terminal fates of B cells (Méndez and Mendoza, 2016) or a dynamical system of only three regulators (Martínez et al., 2012). Larger dynamical models are capable of explaining the distribution of time spans that B cells can spend undergoing somatic hypermutation (SHM) prior to terminal differentiation but either do not include NFκB, cRel, or RelA (Sciammas et al., 2011) or consider NFκB as a single regulator without distinct functions of cRel or RelA (Martínez et al., 2012; Méndez and Mendoza, 2016).

To better understand the role of NFκB within the ASC differentiation circuit, we extended the work of Sciammas et al. (2011) by developing a mathematical model of ASC differentiation in which cRel and RelA are investigated as distinct regulators. Mathematical modeling, combined with mechanistic and functional experimental studies, revealed that cRel must be repressed for ASC differentiation. We showed that decreased cRel expression is

mediated by Blimp1 through epigenetic remodeling of the *Rel* locus. This insight allowed us to integrate the extended ASC differentiation circuit model into our previously established multi-scale model to account for the cell population dynamics of ABCs and ASCs in terms of the dynamics of intra-cellular molecular signaling events.

## RESULTS

### Mathematical Modeling Predicts that cRel Inhibits B Cell Differentiation into ASCs

The previously established ASC differentiation circuit model (Sciammas et al., 2011) includes regulatory interactions between transcription factors IRF4, Pax5, Blimp1, Bach2, and Bcl6 (Figures 1A and 1B). To explore the roles of NFκB dimers in ASC differentiation, we incorporated RelA and cRel and their known dimer-specific regulatory interactions into the ordinary

differential equation (ODE) model of Sciammas et al. (2011): cRel is known to induce IRF4 (Grumont and Gerondakis, 2000), Bach2 (Hunter et al., 2016) and activation-induced deaminase (AID) activity (Kim and Tian, 2009; Park et al., 2009); and RelA induces IRF4 (Saito et al., 2007), Blimp1 (Heise et al., 2014; Morgan et al., 2009) and AID (Park et al., 2009) (Figure 1B and Table S1). The resulting "NFκB-extended ASC model v1" contains 7 molecular species controlled by 14 regulatory interactions (Figure 1B, Table S2, and Data S1).

Time-course simulations showed that ASC differentiation trajectories passed through an obligate transient state of high AID followed by increased Blimp1 and subsequent AID repression to become ASCs (Figure 1C). To interpret model simulations, we defined an ASC as a cell that is Blimp1$^{high}$ and AID$^{low}$ (Blimp1 > 4, consistent with Sciammas et al., 2011, and AID < 4) (Figure S1A). However, simulations using the NFκB-extended ASC model v1 failed to produce ASCs in expected numbers (Figures 1C and 1D). AID and Blimp1 upregulation were consistent with published results, but increased Blimp1 expression was not followed by the obligate AID decrease (Figures 1C and 1D). At face value, this simulation result suggests that either RelA or cRel acts as an inhibitor of ASC differentiation. Given that RelA is required for ASC generation (Heise et al., 2014), we wondered whether decreased cRel expression would allow ABCs that had failed to repress AID to complete their differentiation and become ASCs (Figure 1E). We simulated the effect of decreasing cRel expression (100-, 10-, or 5-fold) in cells that had elevated Blimp1; the model predicted that decreased cRel expression allows for substantial downregulation of AID (Figures 1E, S1B, and S1C), enabling the differentiation of ABCs to ASCs (Figure 1F). This effect was independent of the thresholds chosen to define an ASC (Figure S1A). Thus, math modeling suggested (1) that cRel might be repressed during ASC differentiation and (2) that this regulatory feature might be necessary for ASC generation.

### Transcriptional Repression of *Rel* in ASCs

To test the first model prediction, we generated ABCs and ASCs *ex vivo* by stimulating mature B cells with the TI stimulus lipopolysaccharide (LPS) (Figure S2A) (Kallies et al., 2007). The resulting ASCs showed increased expression of Blimp1 and IRF4 and decreased Bach2 expression compared with expression in ABCs (Figure 2A), confirming that LPS-generated ASCs (defined here as LPS-PBs) can recapitulate key regulatory events of *in vivo* ASCs (Minnich et al., 2016; Nutt et al., 2015; Shapiro-Shelef and Calame, 2005; Shi et al., 2015; Tarlinton et al., 2008). We examined cRel expression by immunoblotting and found that, although both cRel and RelA expression increased during B cell activation, cRel expression decreased ~3.5-fold in LPS-PBs, whereas RelA remained high (Figures 2A and 2B). The same results were observed when PBs were generated with the TD stimulus anti-CD40 and IL-4 (defined as CD40-PBs) (Figures S2B–S2D) (Kallies et al., 2007).

By analyzing deposited RNA-sequencing (RNA-seq) data (Shi et al., 2015), we found that *Rel* mRNA was lower in splenic PBs than in GC B cells and still lower in splenic PCs and bone marrow PCs (Figure S2E). By measuring mRNA with quantitative RT-PCR, we found that *Rel* expression was decreased ~3-fold in LPS-PBs, whereas *Rela* expression remained similar (Figure 2C), and that

*Blimp1* and *IRF4* expression was increased, whereas *Bach2* expression was decreased (Figure S2H). This indicated that cRel repression occurred at the transcriptional level. To validate these observations *in vivo*, we generated ASCs and GC B cells by using immunization with TD antigen (NP-OVA). We purified lymph node-derived ASCs (LN-ASCs) and GC B cells by using flow-cytometry sorting (Figures S2F and S2G). We found that *Rel* transcripts were decreased ~20-fold in LN-ASCs compared with GC B cells, whereas *Rela* remained similar (Figure 2D), and that *Blimp1* and *IRF4* were increased, whereas *Bach2* was decreased (Figure S2I). We also found that cRel expression was decreased in intestinal ASCs (I-ASCs), and these cells showed elevated Blimp1 compared with that in other B cells (Figures S2J and S2K). Altogether, these data suggest that decreased cRel expression could be a general characteristic of PBs and PCs irrespectively of the nature of stimulation and tissue environment.

### Repression of *Rel* Is Required for ASC Differentiation

To test the second model prediction that *Rel* repression is functionally required for ASC differentiation, we used the BCL1 cell line, which is capable of stimulus-responsive differentiation into ASCs, as evident by gene expression signature (Sciammas and Davis, 2004) and antibody production (Lin et al., 1997; Sciammas and Davis, 2004). We found that BCL1 cells stimulated with IL-2 and IL-5 recapitulated the *Rel* repression (Figures S2L and S2M) observed in primary B cells (Figures 2 and S3). We ectopically expressed cRel in BCL1 cells (BCL1-cRel), which elevated Bach2 and diminished Blimp1 proteins (Figure S2M) and increased the proportion of cells in cell cycle (Figure S2N). Similarly, *Bach2* transcript was increased (~2.5-fold) and *Blimp1* transcript was diminished (~1.6-fold) (Figures 2E and 2F), indicating transcriptional control. However, ectopic expression of cRel also diminished the increase in *Blimp1* after stimulation (~1.7-fold, compared with ~3-fold in controls) (Figure 2F). We also found that BCL1-cRel cells failed to produce immunoglobulin M (IgM) upon stimulation (Figure 2G) and did not show a substantial reduction in the proportion of actively cycling cells (~32% compared with ~35% in unstimulated cells) (Figure S2N). Thus, ectopic expression of cRel appears to block terminal differentiation of B cells.

It has been shown that *Bach2$^{-/-}$* B cells have higher Blimp1 and a higher propensity to differentiate into ASCs than WT controls (Muto et al., 2010). We wondered whether the failure to increase Blimp1 expression in BCL1-cRel cells is mediated by Bach2. We deleted *Bach2* in BCL1-cRel cells (Figure S2O) by using CRISPR/Cas9, which reverted *Blimp1* expression to the same level as in control BCL1 cells (Figure 2H) and allowed for differentiation to ASCs, as evident by a rescue of IgM production (Figure 2I). We concluded that for ASC differentiation to proceed, *Rel* must be repressed for expression of *Bach2* to decay and thus for *Blimp1* to be de-repressed.

### Blimp1 Mediates Transcriptional Repression of *Rel*

Given that our computational and experimental studies indicated that decreased cRel expression is required for ASC production, we wondered whether Blimp1 might transcriptionally repress *Rel*. In "NFκB-extended ASC model v2" (Figure 3A), we tested whether an inhibitory connection between Blimp1 and cRel production was sufficient to account for ASC generation
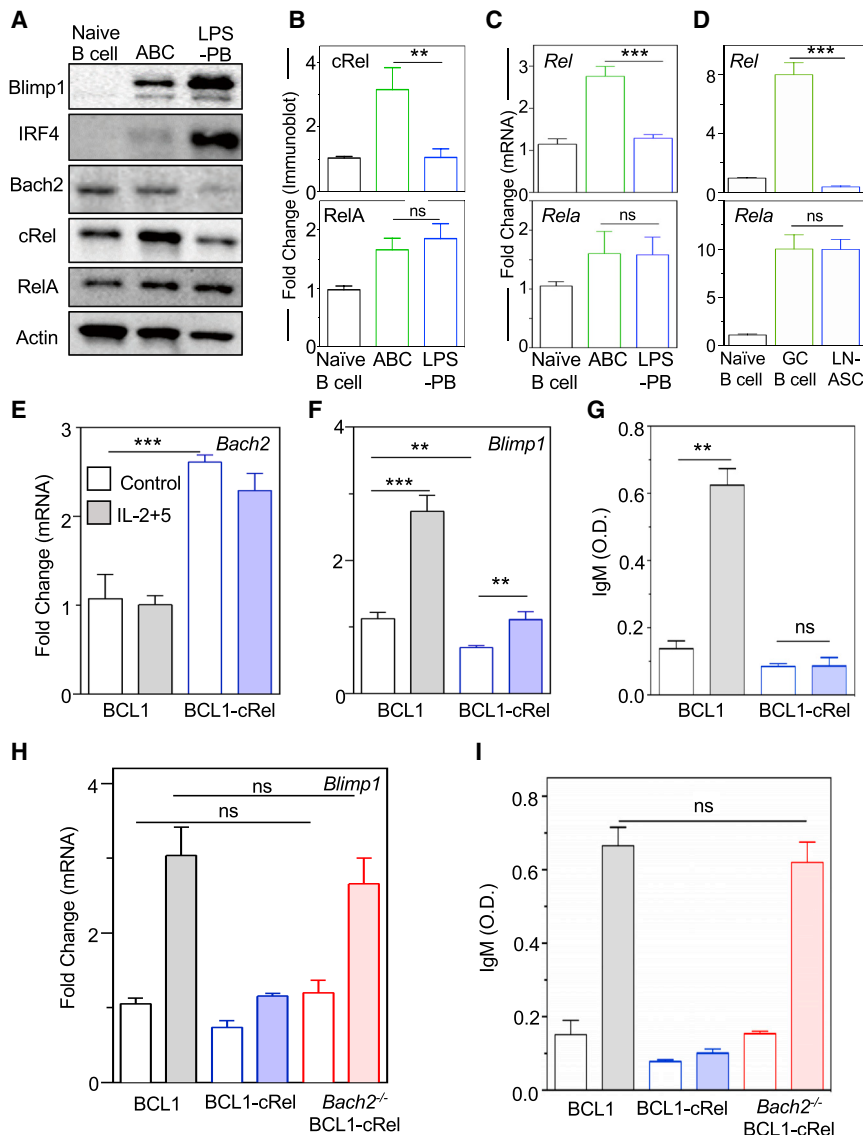
**Figure 2. cRel Repression Is Required for ASC Differentiation**

(A) Immunoblots of Blimp1, IRF4, Bach2, cRel (product of *Rel*), RelA, and actin in naïve B cells, ABCs, and LPS-PBs. ABCs and LPS-PBs were generated by stimulation of naïve B cells with LPS for 72 h and then isolated by flow cytometry (described in Figure S2A). Data shown are representative of 3 biological replicates.

(B) Quantitative measurements of cRel and RelA immunoblots with actin as loading control.

(C) Quantitative measurements of mRNA expression by qPCR of *Rel* (encodes cRel) and *Rela* in naïve B cells, ABCs, and LPS-PBs.

(D) Quantitative measurements of mRNA expression of *Rel* and *Rela* in naïve B cells, GC B cells, and LN-ASCs. *Ubiquitin C* was used as housekeeping gene for quantitation of mRNA expression.

(E and F) Quantitative measurements of mRNA expression of *Bach2* (E) and *Blimp1* (F) in unstimulated (control, blank) and stimulated (IL-2 + IL-5 for 24 h, shaded) BCL1 cells (gray) and cRel-overexpressing BCL1 cells (blue, BCL1-cRel). IL-2 and IL-5 (shaded) stimulation is used throughout to differentiate BCL1 cells to ASC-like states.

(G) IgM production measured at 96 h by ELISA and expressed in optical density (OD) units.

(H) Quantitative measurement of mRNA expression of *Blimp1* in unstimulated (control, blank) and stimulated (IL-2 + IL-5 for 24 h, shaded) BCL1 (gray), BCL1-cRel (blue), and Bach2-KO BCL1-cRel (red) cells.

(I) IgM production measured at 96 h by ELISA and expressed in OD units.

In all plots, the mean and SD of 3 replicates are indicated. *p < 0.05, **p < 0.01, ***p < 0.001, and not significant, ns (unpaired Student's t test).

quantitatively. Indeed, the model recapitulated experimental flow-cytometry results (Figures 3B and 3C) within a broad range of Blimp1 and AID thresholds used to define ASCs (Figure S3). Thus, the mathematical model predicted that Blimp1-mediated repression of *Rel* might be sufficient to allow ASC differentiation.

To experimentally test whether Blimp1 triggers repression of *Rel*, we deleted *Blimp1* in BCL1 cells (Figure S4A) and measured *Rel* transcripts upon stimulation. Whereas control BCL1 cells showed a ~4-fold decrease in *Rel* expression in response to stimulation with IL-2 and IL-5, *Blimp1*-deleted BCL1 cells failed to repress *Rel* upon stimulation (Figure 4A), and *Rela* expression remained largely unchanged (Figure 4B). *Blimp1*-deleted BCL1 cells were unable to proceed with ASC differentiation, as evident by the lack of IgM production (Figure 4C). Further, by analyzing RNA-seq data of primary B cells (Tellier et al., 2016), we found that *Blimp1*$^{-/-}$ PCs showed increased expression of *Rel* (Figure S4B). This indicated that Blimp1 represses *Rel* expression as part of its program to coordinate ASC differentiation.

To establish whether Blimp1-mediated transcriptional repression of *Rel* is direct, we examined recently deposited Blimp1 ChIP-seq data from PBs (Minnich et al., 2016) and found a prominent Blimp1 binding peak in the *Rel* locus at position ~23,669,376–23,670,485 in chromosome 11 by using genome assembly mouse mm9 (Figure 4D). Whereas BCL1 cells showed a ~4-fold transcriptional repression of *Rel* in response to stimuli, CRISPR/Cas9-mediated disruption of a Blimp1 binding site in the *Rel* locus (*Rel*$^{BBS}$; Figure S4C) substantially reduced this repression (Figure 4E). *Rela* expression remained unchanged in either cell line (Figure 4F). As expected, the *Rel*$^{BBS}$ mutation rendered BCL1 cells unable to fully proceed with ASC differentiation, as made evident by reduced IgM production (Figure 4G). Thus, we concluded that Blimp1 directly represses *Rel* expression in ASCs.

Next, we sought to characterize the mechanism by which Blimp1 represses *Rel* transcription. Blimp1 is known to interact with histone deacetylases (e.g., HDAC2) and was shown to repress transcription by recruiting HDACs to a target promoter (Yu et al., 2000), reducing H3K9 acetylation (H3K9ac) abundance (Minnich et al., 2016). We measured H3K9ac abundance on the *Rel* locus in ABCs and LPS-PBs by ChIP-qPCR and found a
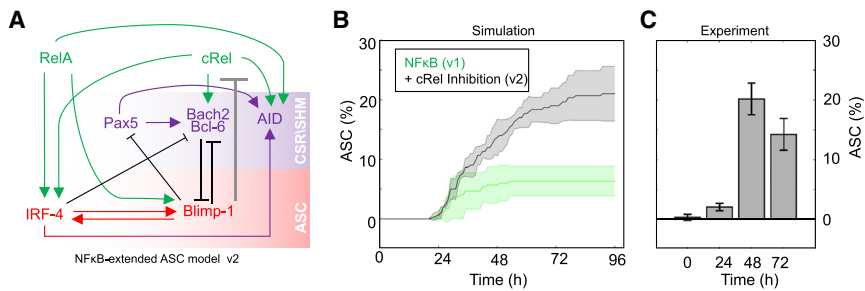
**Figure 3. Including Blimp1 Inhibition of cRel Expression in Computational Simulations Enables ASC Differentiation**

(A) Schematic of NFκB-extended ASC differentiation model v2, in which cRel downregulation was initiated by Blimp1 (gray barred line).

(B) Percentage of ASC production over time (h) in simulations with model v1 (without cRel-Blimp1 inhibition, green, Figure 1B) and v2 (with cRel-Blimp1 inhibition, gray, A). The solid line indicates the mean, and the shaded region indicates the SD of 3 simulations, each containing 125 founder cells.

(C) Experimental measures of the ASC differentiation kinetics determined by flow cytometry at 24, 48, 72, and 96 h; the mean and SD of 3 replicates are indicated.

~1.4% ± 0.108% yield in ABCs as opposed to ~0.4% ± 0.026% yield (relative to input) in LPS-PBs, whereas antibody isotype controls were low (~0.05%) and unchanged (Figure S4D). This reduction in H3K9ac by more than 3-fold on the *Rel* locus as ABCs differentiated into LPS-PBs contrasted with unchanged H3K9ac at ~1.9% ± 0.1% on the *Rela* locus (Figure S4E). Similarly, ChIP-seq data (Minnich et al., 2016) showed reduced H3K9ac at the *Rel* locus (Figure S4F). Upon stimulation of BCL1 cells with IL-2 and IL-5, we found a ~2.6-fold decrease in H3K9ac on the *Rel* locus in control cells (from ~1.7% ± 0.19% to 0.64% ± 0.1%) but no significant change in *Blimp1*−/− cells (from ~1.84% ± 0.19% to 1.8% ± 0.2%) (Figure 4H). Similarly, mutation of the Blimp1 binding site (*Rel*BBS) substantially diminished the loss of H3K9ac abundance in response to stimulus (~1.45% ± 0.11%) at the *Rel* locus compared with that in controls (0.64% ± 0.1%) (Figure 4H) but had no impact at the *Rela* locus (Figure 4I). Thus, we concluded that the differentiation-associated reduction of H3K9ac abundance at the *Rel* locus is dependent on direct binding of Blimp1 and leads to transcriptional repression of *Rel* in ASCs.

## cRel Deficiency Increases the ASC Differentiation Propensity but Results in a Smaller ASC Population

To further test the regulatory mechanisms encapsulated in the computational model, we simulated ASC generation in the absence of cRel and found that the model predicted an increase in ASC numbers at time points after 48 h (Figure 5A). This prediction was independent of the threshold of Blimp1 and AID chosen to define a cell as an ASC (Figure S5A) and consistent with a previous report that *Rel*−/− B cells produce a higher percentage of ASCs after 3 days than WT controls (Heise et al., 2014). In our experiments, we found that although *Rel*−/− B cells had a substantial proliferative defect and thus generated fewer cells overall than did WT cells (Figure 5B), the culture contained −1%, −2%, +20%, and +15% greater proportion of LPS-PBs than WT controls at 24, 48, 72, and 96 h, respectively (Figures 5C and S5B). By measuring the cell loss associated with cRel deficiency, we found that the increased loss in the ABC population from 48 to 72 h (88% to 97%) coincided with a decreased loss of LPS-PBs from 48 to 72 h (91% to 86%) (Figure S5C). We also measured cell-death propensities with annexin V staining and found that ABCs and LPS-PBs generated from *Rel*−/− B cells showed a similar ~2-fold higher rate of cell death than did those generated from WT B cells (Figures S5D and S5E). These data

suggest that the increased proportion of LPS-PBs versus ABCs in *Rel*−/− B cells is not due to differential death rates, but rather due to an increased propensity to differentiate from ABCs into ASCs. These results show a quantitative agreement with computational predictions (Figure 5A), except for the last time point, which could reflect a limitation of the *in vitro* culture conditions.

To further test the regulatory connections in the model, we generated quantitative predictions of the dynamic changes of three critical regulators (Blimp1, Bach2, and IRF4) after stimulation of *Rel*−/− versus WT B cells. In the mutant, we predicted a 2-fold late-phase increase in Blimp1, a 2- to 3-fold reduction in Bach2, and an initial decrease in IRF4 followed by a late-phase increase (Figure 5D). Experimental quantification by RT-PCR showed a quantitative match to the computational prediction such that *Rel*−/− B cells, compared with WT controls, had 2-fold higher expression of *Blimp1* in the late-phase, 2- to 3-fold lower expression of *Bach2*, and similarly dynamic regulation of *IRF4* (Figures 5E and S5F). Immunoblots showed similar trends as observed by RT-PCR (Figure 5F). Thus, *Rel*−/− B cells had a higher propensity to differentiate into ASCs through increased expression of Blimp1 than did WT B cells.

Given that ASC generation propensity has been shown to increase with cell division (Hasbold et al., 2004), we wondered whether *Rel*−/− B cells have an increased ASC differentiation propensity in a generation-specific manner. Cell division was measured by dye dilution assay using Cell Trace Red. Although both WT and *Rel*−/− B cells showed increasing ASC generation with each division, *Rel*−/− B cells showed a higher proportion of non-dividing (generation "0") cells and an increased proportion of LPS-PBs at every generation (Figures 5G and 5H). Thus, *Rel*−/− B cells showed higher ASC differentiation propensities at all generations than did WT B cells.

## Integrating the ASC Differentiation Circuit into a Multi-scale B Cell Proliferation Model Reveals How cRel Dynamics Control the Dynamics of Distinct B Cell Populations

The link between differentiation and division revealed in the WT and *Rel*−/− B cell experiments motivated us to integrate the "NFκB-extended ASC model v2" into an established multi-scale model that accounts for B cell population dynamics as a result of the molecular network in each cell (Mitchell et al., 2018; Shokhirev et al., 2015). By doing this, we could discover whether
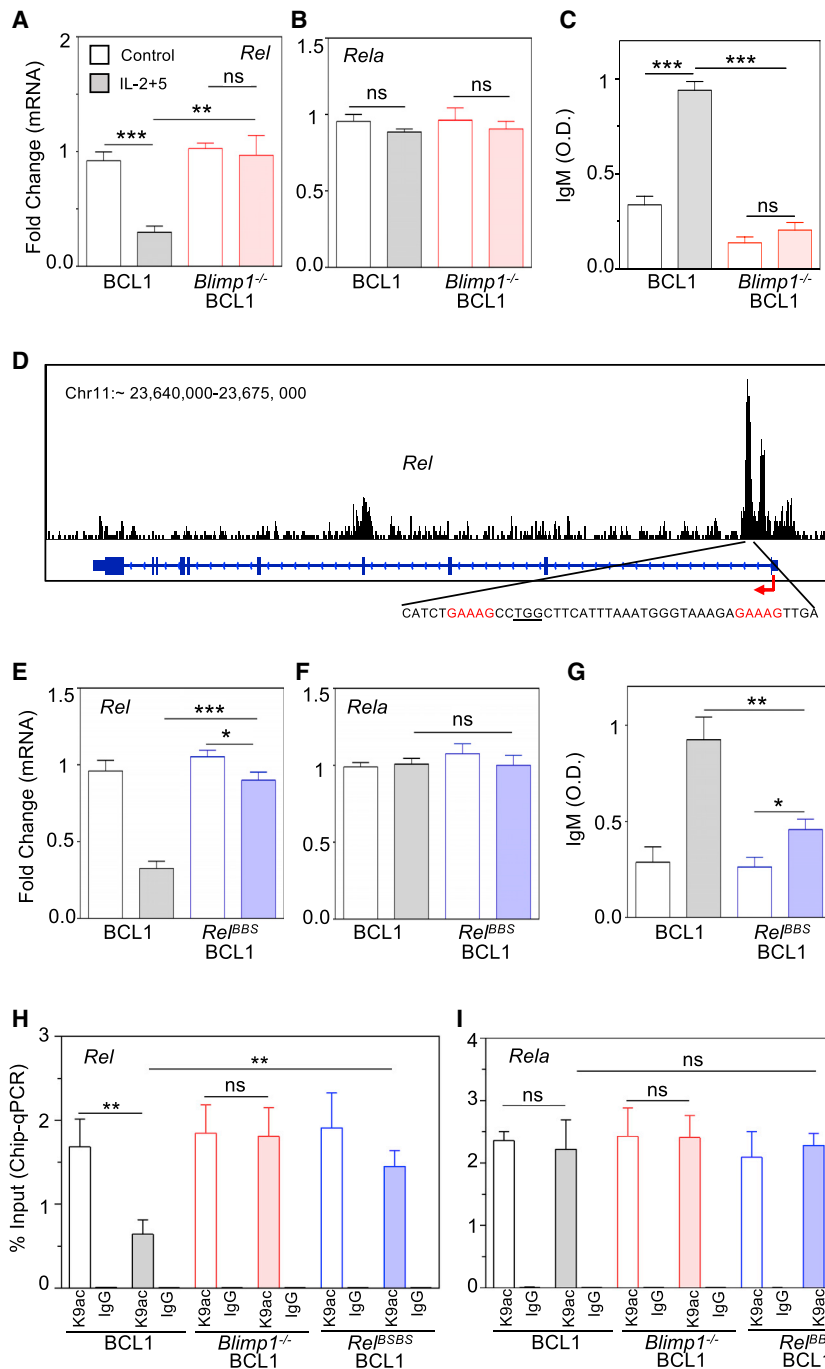
**Figure 4. Blimp1 Represses *Rel* Expression and Diminishes H3K9ac at the *Rel* Locus**

(A and B) Quantitative mRNA expression by qPCR of *Rel* (A) and *Rela* (B) in unstimulated (control, blank) and stimulated (IL-2 + IL-5 for 24 h, shaded) BCL1 (gray) and *Blimp1*−/− BCL1 (red) cells.

(C) IgM production measured at 96 h by ELISA and expressed in OD units.

(D) Analysis of Blimp1 ChIP-seq data in plasmablasts (GEO: GSM1843340; Minnich et al., 2016). Shown are the Blimp1 binding track (top), schematic of the *Rel* locus (middle), consensus-Blimp1-binding motif (red, bottom), and targeted PAM sequence (underlined, bottom).

(E and F) Quantitative mRNA expression of *Rel* (E) and *Rela* (F) in unstimulated (control, blank) and stimulated (IL-2 + IL-5 for 24 h, shaded) BCL1 (gray) and *Rel*BBS BCL1 cells (BCL1 cells mutated at the Blimp1 binding site in the *Rel* locus, blue).

(G) IgM production was measured at 96 h by ELISA and expressed in OD units.

(H and I) ChIP-qPCR yield for H3K9ac and IgG (isotype control) at the *Rel* locus (H) and *Rela* locus (I) in unstimulated (control, blank) and stimulated (IL-2 + IL-5 for 24 h, shaded) BCL1 (gray), *Blimp1*−/− BCL1 (red), and *Rel*BBS BCL1 (blue) cells. The yield was calculated with respect to input.

The mean and SD of 3 replicates are shown throughout. *p < 0.05, **p < 0.01, ***p < 0.001, and not significant, ns (unpaired Student's t test).

ASC (Figure 6B), and cell-fate decisions were dependent on the particular parameter set sampled from previously determined distributions (see STAR Methods; Mitchell et al., 2018).

A simulation was performed of 200 seeded cells stimulated with LPS. Dynamic changes of cRel activation were measured over time as cells within each lineage transition from ABCs (Blimp1low) to Blimp1highAIDhigh and subsequently to ASCs (Blimp1highAIDlow). As expected, the model showed almost immediate cRel activation and resulting proliferation. Only cells that had increased Blimp1 expression showed decreased cRel activity, and they showed further decreases at later time points as they differentiated into ASCs (Figure 6C), whereas RelA activity remained similar in ABCs and

our mechanistic understanding was sufficient to explain the effects we observed on differentiation and proliferation and the link between the two. This multi-scale model includes an NFκB module that predicts NFκB-dimer-specific dynamics as a result of the stimulus-induced regulation of multiple inhibitors of NFκB (IκBs). We added NFκB's control over ASC differentiation, as described here in "NFκB-extended ASC model v2," to existing NFκB-mediated control over the cell cycle and apoptosis (Figure 6A). Each cell within this multi-scale model was thus capable of undergoing apoptosis, cell division, or differentiation into an

ASCs (Figure S6A). According to parameter distributions, cells showed heterogeneity in cRel activation dynamics and the timing and generation number of ASC differentiation (Figure 6C). The model predicted that ASCs generated at early time points produced a higher percentage of proliferating cells than did those generated at a later time point (Figures 6D and S6B).

To examine the time evolution of molecular markers and generate an experimentally testable prediction of the multi-scale modeling of signaling, proliferation, apoptosis, and differentiation, we tracked cRel and Blimp1 concentrations over time in a
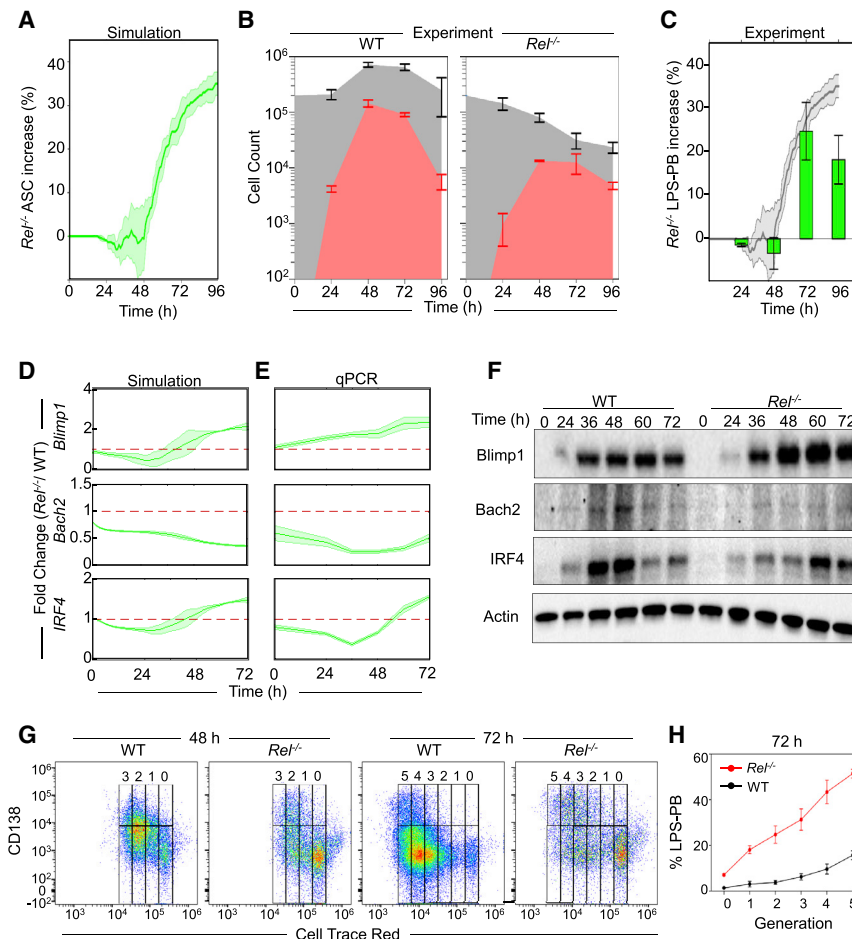
**Figure 5. cRel Deficiency Enhances ASC Differentiation**

(A) Time-course plot of the percentage (%) increase of ASCs in cRel-deficient ($Rel^{-/-}$) B cells compared with WT controls, as predicted by mathematical modeling using the NFκB-extended ASC differentiation model v2. The percentage of LPS-PBs is plotted with time (h). The solid line indicates the mean, and the shaded region indicates the SD of 3 replicates with 125 initial cells.

(B) Stacked-area plot indicates experimentally determined absolute cell numbers at 0, 24, 48, 72, and 96 h upon stimulation of WT (left) and $Rel^{-/-}$ (right) B cells with LPS. Gray plot indicates total cell number (ABCs and LPS-PBs), and the red area indicates the number of LPS-PBs.

(C) Bar graph showing the percentage increase of LPS-PBs over WT in $Rel^{-/-}$ B cells as measured by flow cytometry from WT and $Rel^{-/-}$ B cells at 24, 48, 72, and 96 h. The LPS-PBs percentage is determined by B220$^{lo}$CD138$^+$ (described in Figure S5B). The model prediction (A) is reproduced as the shaded gray region behind the bar graph.

(D and E) $Blimp1$, $Bach2$, and $IRF4$ fold change in $Rel^{-/-}$ B cells compared with WT B cells over time, as predicted by mathematical modeling (left) and determined experimentally by qPCR (right). The solid line indicates mean, and the shaded region indicates the SD of fold change from 3 replicates (y axis) over time (x axis). No change over WT (fold change = 1) is indicated with a red dashed line. The mean and SD of 3 replicates are shown throughout.

(F) Representative immunoblots of Blimp1, Bach2, IRF4, and actin expression in $Rel^{-/-}$ and WT B cells. Immunoblots were performed at 0, 24, 36, 48, 60, and 72 h after stimulation with LPS.

(G) Flow-cytometry plot of ASCs (CD138$^{high}$) and ABCs (CD138$^{-/low}$) at each generation (Cell Trace Red) during LPS-PB production in WT and $Rel^{-/-}$ B cell at 48 and 72 h. The generation number is indicated at the top of each plot. A representative of 3 replicates is shown.

(H) Percentage of LPS-PBs at each generation in WT (red) and $Rel^{-/-}$ (black) B cells at 72 h. The x axis indicates generation number, and the y axis indicates LPS-PB percentage. The mean and SD of 3 replicates are shown throughout.

population of individually simulated cells (Figure 6E and Video S1). The resulting plot of the cell population's path through the space of cRel and Blimp1 expression revealed a distinctive trajectory that allowed us to quantify specific populations of B cells on the basis of their cRel and Blimp1 expression (Figure 6F). To test this prediction, we measured Blimp1 and cRel abundance with single-cell resolution through a flow-cytometry time course and found that B cells first increased cRel expression at 24 h, and ∼70% of cells were considered cRel$^{high}$ at 24 and 48 h (Figures 6G and 6H). Increased cRel expression was followed by increased Blimp1 expression, such that the percentage of Blimp1$^{high}$ cells increased from 20% at 24 h to 55% at 48 h and ∼80% at 72 and 96 h. As predicted by the model, B cells that showed increased Blimp1 subsequently reduced cRel expression, whereby the percentage of cells with both high Blimp1 and high cRel decreased from 41% at 48 hr to 29% at 72 hr and 22% at 96 hr, and the population of cells with high Blimp1 and low cRel increased from 15% at 48 hr to 53% at 72 and 96 hr. This confirmed the computational prediction that proliferation and differentiation dynamics of stimulated B cells

are accompanied by first high and then decreased cRel expression after increased expression of Blimp1 at 72 and 96 h (Figures 6G and 6H).

## Multi-scale Modeling Relates Genetic Perturbations to Physiological or Pathological B Cell Population Dynamics

To further investigate the predictive power of the multi-scale model, we examined its ability to recapitulate population dynamics of WT and $Rel^{-/-}$ B cells. In the WT condition (Figure 7A, left), the model simulations showed a characteristic transient dip in the total population as a result of the death of a proportion of founder cells before proliferation results in a total population expansion that then gives way to a population decline. During the proliferative burst, some cells differentiated into ASCs, resulting in ASC population dynamics that are distinct but necessarily coordinated with the ABC population dynamics. In the $Rel^{-/-}$ simulation (Figure 7A, right), the total population expansion was dramatically diminished (in agreement with experimental literature; Köntgen et al., 1995; Shokhirev et al.,
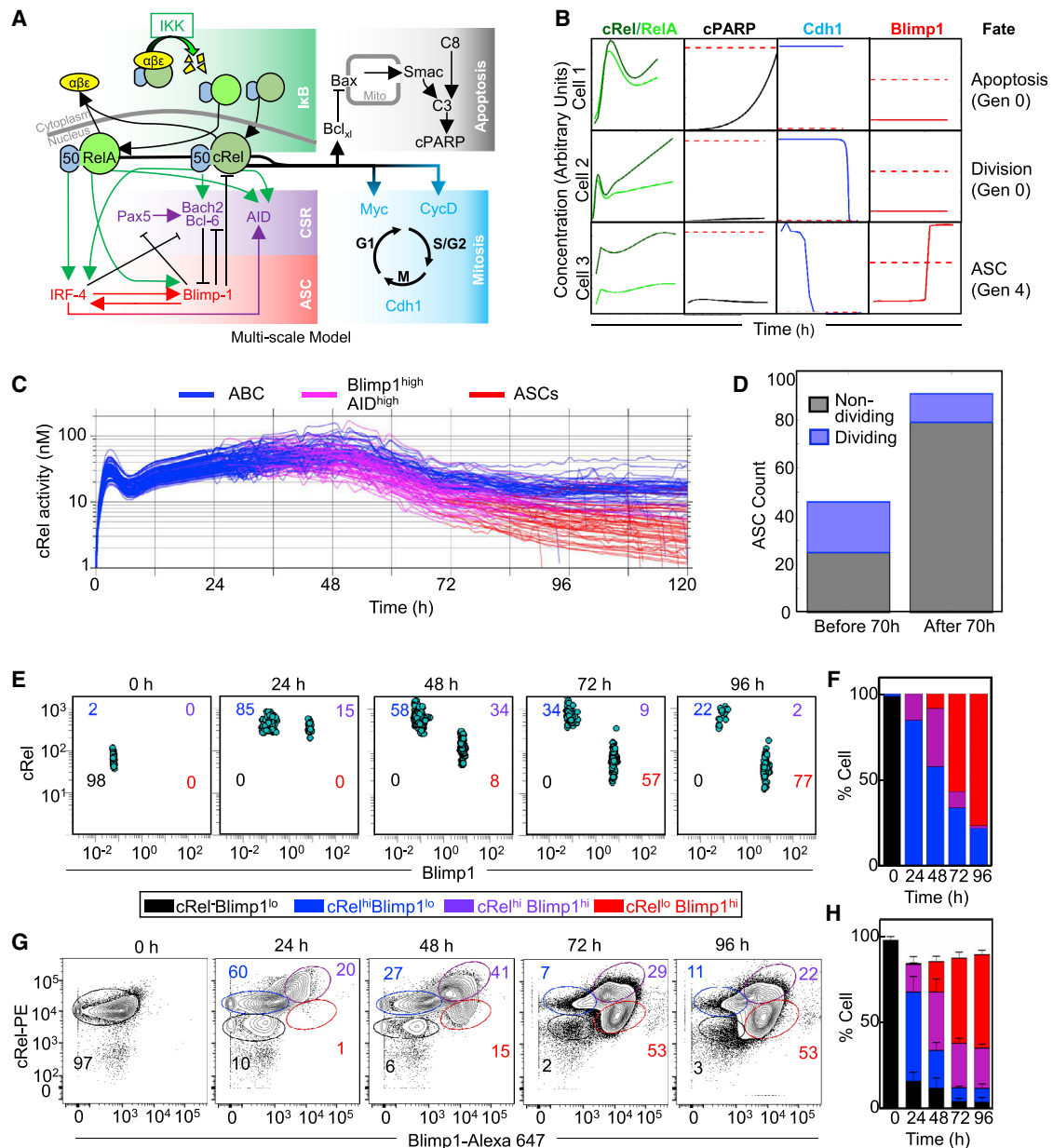
**Figure 6. Dynamic cRel Repression Is Initiated by Blimp1 in Single Cells**

(A) Schematic of multi-scale modeling that determines B cell population fate dynamics with single-cell resolution. The multi-scale model is composed of the NFκB regulatory network (green box), the apoptosis gene regulatory network (gray box), the cell-cycle gene regulatory network (blue box) as published previously (Mitchell et al., 2018; Shokhirev et al., 2015), and the ASC differentiation circuit (violet and red box) added here.

(B) Line plots indicate dynamics of NFκB, cPARP, Cdh1, and Blimp1 in 3 representative cells. Thresholds that trigger fate changes are indicated with red dashed lines. Exceeding the threshold of cPARP triggers apoptosis (cell 1), Cdh1 triggers mitosis (cells 2 and 3), and Blimp1 triggers differentiation into an ASC (cell 3). Thresholds must be crossed in the positive direction. Cells 1 and 2 are founder cells (generation 0), whereas cell 3 has undergone 4 divisions (generation 4).

(C) Line plots of average cRel activity (nuclear cRel:p50 concentration) within 200 simulated lineages. Each line represents the average concentration of progeny from a single founder cell. ASC-generating lineages are indicated as ABCs (blue) transition to Blimp1^{high}AID[high] (pink) and ASCs (red). The x axis indicates time (h), and the y axis indicates simulated nuclear cRel-p50 heterodimer in nanomolar (nM).

(D) Stacked bar graph of the number of ASCs that would not divide (black) and those that underwent at least one division after differentiating (blue). Bars are shown for ASCs generated before and after 70 h.

(E) Blimp1 and cRel expression in a population of 1,000 single cells simulated with the multi-scale model (A) at 0, 24, 48, 72, and 96 h. Populations were gated into cRel⁻Blimp1^{low} (black), cRel[high]Blimp1^{low} (blue), cRel[high]Blimp1⁺ (violet), and cRel[low]Blimp1⁺ (red). Cell numbers are indicated in each quadrant. Time points at 15 min time intervals are shown in Video S1.

(F) Stacked bar graph of the percentage of cells in each quadrant in the simulation (E) at the indicated time points.
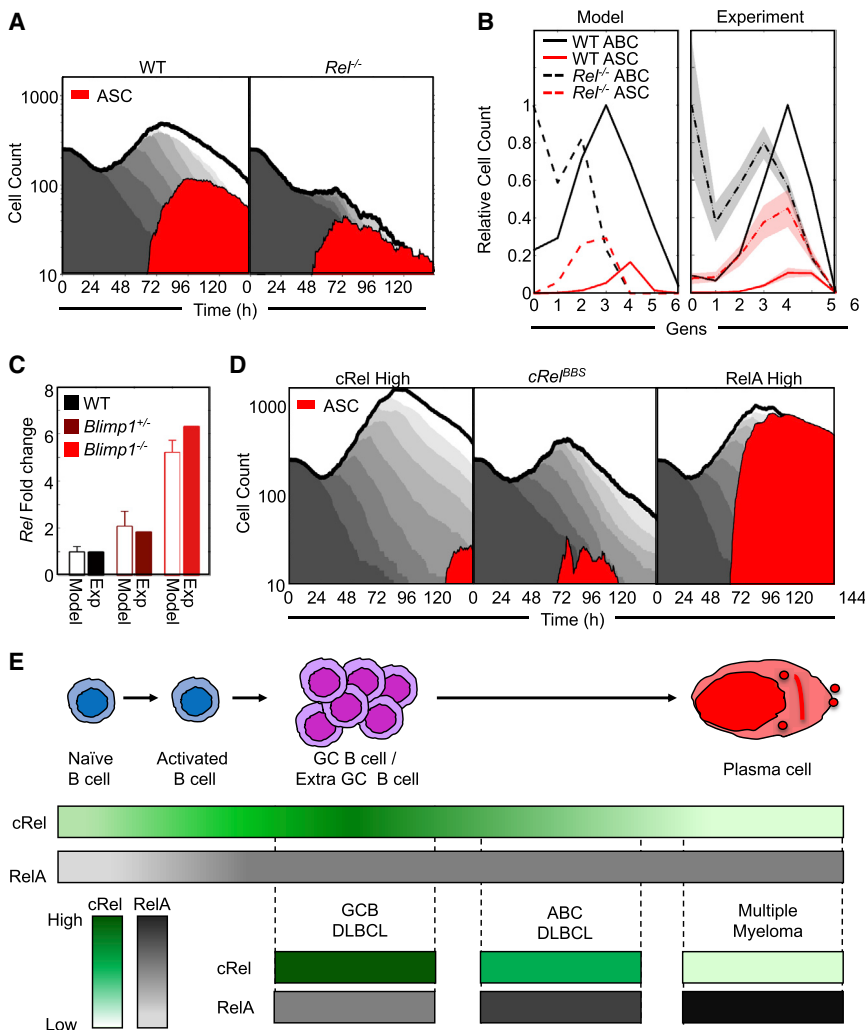
*(legend continued on next page)*

**Figure 7. Coordinated cRel and RelA Dynamics Control the Dynamics of B Cell Populations**

(A) Area plots from multi-scale modeling simulations of 125 WT and $Rel^{-/-}$ cells show total cell number (gray) and ASC populations (Blimp1$^{high}$AID$^{low}$, red). Each subsequent generation of proliferating cells is indicated with a lighter gray.

(B) Line graphs showing generation-specific cell counts of ABCs (black) and ASCs (red) in WT (solid line) and $Rel^{-/-}$ (dashed line) simulations (left) and experiment (right, Figure 5G). Cell counts are normalized to the maximum cell count of ABCs for each genotype. The shaded region shows the SD of 3 experimental replicates.

(C) Bar graph of the fold change of cRel expression over WT (black), $Blimp1^{+/-}$ (maroon), and $Blimp1^{-/-}$ (red) B cells in simulations and experiment (details of experimental data are shown in Figure S7).

(D) Area plots from multi-scale modeling simulations of 125 cRel$^{high}$ (left), $Rel^{BBS}$ (middle), and RelA$^{high}$ (right) cells show total cell number (gray) and ASC populations (Blimp1$^{high}$AID$^{low}$, red). Each subsequent generation of proliferating cells is indicated with a lighter gray.

(E) Illustration of cRel and RelA dynamics during the physiological B cell response and their characteristic abundances in B cell malignancies. Top: during B cell differentiation, naive B cells produce ABCs, followed by GC B cells, before differentiating into PCs. Middle: color graph to represent expression of cRel (green) and RelA (gray) during the stages of B cell differentiation. Color gradient represents relative expression, and darker colors indicate higher expression. Bottom: cRel and RelA expression characteristic of indicated B cell malignancies. Their putative cell of origin is indicated by alignment with the upper panel.

2015). Although the ASC population was also diminished, their proportion of the total was substantially higher in the cRel-deficient population than in WT controls, reflecting the enhanced propensity to differentiate (Figures 7A and 5B). By analyzing the simulation data not as a function of time but as a function of generation at a single time point (72 h), we found that the model predicted that cRel-deficiency results in an overall increase in ASC differentiation, which in fact peaks at an earlier generation than in WT cells (Figure 7B, left). The experimental data (Figure 5G) confirmed this prediction (Figure 7B, right), though peak ASC proportions appeared one generation later in both genotypes. In sum, the multi-scale model appeared to recapitulate key aspects of ABC and ASC population dynamics and the intricate roles of cRel in shaping them.

The concordance between model simulations and experimental observations encouraged us to use the multi-scale model

as a research tool to explore the consequence of NFκB dysregulation on B cell population dynamics. Simulations of Blimp1 deficiency resulted in increased $Rel$ expression (Figure 7C) and elevated B cell proliferation (Figure S7) in line with experimental observation (Calado et al., 2010). Simulation of elevated cRel expression resulted in a dramatic increase in the expansion of the ABC population and a reduction and delay in the generation of ASCs not only proportionally but also in absolute numbers (Figure 7D, left), reflecting experimental observations (Figure 2G). Next, we simulated the effects of disrupting the Blimp1 binding sites in the $Rel$ locus, which did not substantially alter total ABC cell population dynamics but did result in a reduction in the generation of ASCs (Figure 7D, middle). This was consistent with the reduced antibody production observed experimentally (Figure 4G). Finally, we explored the effect of elevated RelA expression, which led to increased total cell population

(G) Blimp1 and cRel expression measured by flow cytometry with single-cell resolution at 0, 24, 48, 72, and 96 h. Populations were gated into cRel$^-$Blimp1$^{low}$ (black), cRel$^{high}$Blimp1$^{low}$ (blue), cRel$^{high}$Blimp1$^+$ (violet), and cRel$^{low}$Blimp1$^+$ (red). The percentage of cells in each gate is represented by a number in each plot with the respective color code.

(H) Stacked bar graph of the percentage of cells in each gate at the indicated time points (G). The mean and SD of 3 replicates are indicated.

expansion, comparable to elevated cRel simulations. But, in contrast to the elevated cRel condition, elevated RelA produced predominantly ASCs (Figure 7D, right).

Similar misregulation of the NFκB system is associated with different B cell lymphomas originating from distinct phases of the GC reaction (Figure 7E). GC B-cell-like diffuse large cell lymphomas (GCB DLBCLs) are associated with high cRel expression, and similar to the cRel[high] simulations, GCB DLBCL cells appear trapped at the cRel[high] stage and unable to exit the GC (Rosenwald et al., 2002; Shaffer et al., 2002b). Activated B-cell-like diffuse large cell lymphomas (ABC-DLBCLs) show high RelA and moderately high cRel activity with frequent Blimp1 inactivation. As seen in the Blimp1 deficiency simulation, such cells are trapped at the pre-plasmablast stage (i.e., able to initiate but unable to complete plasmacytic differentiation) (Davis et al., 2001). In contrast, malignant plasma cell disorder multiple myeloma (MM) is characterized by high RelA, and reflecting the highly differentiated state of cells in RelA high simulations, MM cells originate from fully differentiated plasma cells. The fact that our simulations of conditions of NFκB misregulation produced analogous *in silico* phenotypes of population dynamics (Figure 7C) suggests that the multi-scale model might be a useful research tool for relating genetic or molecular perturbations to the balance of proliferation and differentiation in health and disease.

## DISCUSSION

In this work, we developed a quantitative understanding of how NFκB dimers control ASC differentiation; by iterating experimental and computational modeling work, we formulated an experimentally trained kinetic model of B cell proliferation and differentiation, which recapitulated experimentally observed phenotypes. Although cRel activation is critical for B cell activation and survival and ABC population expansion (Pohl et al., 2002; Shokhirev et al., 2015), we found that its repression enabled differentiation of ABCs into ASCs. Ectopic expression of cRel in B cells prevented Blimp1 expression and consequently impaired ASC differentiation. Conversely, *Rel*^{−/−} B cells showed increased Blimp1 expression and increased propensity for LPS-PB differentiation, but the LPS-PB population remained diminished, suggesting that the reduced antigen-specific antibody production (Grumont and Gerondakis, 2000; Heise et al., 2014; Pohl et al., 2002) associated with cRel deficiency is not due to a defect in ASC generation but rather an indirect consequence of defective B cell expansion. Thus, cRel dynamics are a key determinant of ABC and ASC population dynamics.

Further, we established that *Rel* repression in ASCs is mediated by Blimp1. Blimp1 is known to repress cell-growth and -proliferation regulators such as Myc and cyclin E (Lin et al., 2000; Lin et al., 1997; Shaffer et al., 2002a); *Rel* repression might reinforce this regulation as Myc is a cRel target gene (Duyao et al., 1990), which was shown to determine the proliferative capacity of ABCs (Heinzel et al., 2017). A key characteristic of plasma cells is the slowing and cessation of the cell cycle, and ectopic expression of the cell-cycle-promoting regulator (cyclin E) inhibits ASC differentiation (Lin et al., 2000). cRel expression also correlates with proliferative activity (Alves et al., 2014; Heinzel et al., 2017), and cycling PBs show less cRel downregulation

than quiescent PCs. Future studies might address to what extent cRel expression determines proliferative capacity of ABCs.

Our work points to a mutually antagonistic regulatory logic between cRel and Blimp1, where cRel inhibits Blimp1 expression via Bach2 and Blimp1 directly represses cRel expression. Mutual inhibition within regulatory networks can result in a bi-stable system, i.e., a system with two steady states (Kaplan and Glass, 2012). Here, one state was characterized by Blimp1^{low}cRel[high] and another by Blimp1^{high}cRel[low]. Further, our work suggests that ABC and ASC population dynamics are governed by how cells dynamically transition through the state space. Stimulation of B cells does not only activate cRel but also RelA, which (directly and through IRF4) promote Blimp1 expression; this then allows a portion of cells to build up sufficient Blimp1 to transition to the Blimp1^{high}cRel[low] state and differentiate into ASCs. Thus, in the context of B cell proliferation and differentiation, cRel and RelA do not compensate for each other (Hoffmann et al., 2003), but they have distinct, potentially antagonistic functions. We posit that the coordinated dynamic control of these two NFκB family members, and their relative activity over time, phase the GC reaction of B cell population expansion, SHM, and ASC generation for an effective immune response.

Bi-stable systems might enforce differentiation decisions so that the differentiated state of the cell is maintained even when the differentiating stimulus has decayed (Wang et al., 2009). Healthy ASC differentiation is indeed irreversible, and only a significant perturbation of regulatory networks, such as the overexpression of Bcl6, might lead to deactivation of the ASC-specific gene expression program (Fujita et al., 2004). Although various ASC populations, such as PBs, PCs, and ASCs, from distinct niches show variable Blimp1 and cRel abundances, the mutual antagonistic regulation between Blimp1 and cRel might be conserved. Indeed, we found that as Blimp1 expression gradually increases from PBs to PCs, there is a concomitant decrease in cRel. An inverse correlation between Blimp1 and cRel expression was also observed in intestinal B cells and I-ASCs and in human pre-plasma cells exiting from the GC (Cattoretti et al., 2005). Nevertheless, the Blimp1 transcriptional repression program might differ in other ways in distinct ASC populations; for example, I-ASCs fail to repress the Blimp1 target gene CD19 (Landsverk et al., 2017), and ASC differentiation during *Salmonella* infections might involve a prolonged Blimp1^{high}AID[high] state resulting in GC-independent affinity maturation of PBs and pathological B cell responses (Di Niro et al., 2015).

Here, we presented a mathematical model (NFκB-extended ASC model v.2), which demonstrated that the included gene regulatory interactions are sufficient to explain the differentiation kinetics and regulatory dynamics explored here. However, other *in vivo* or *ex vivo* experimental conditions might involve additional mechanisms. For example, recent results revealed a significant role for the complex of IRF8 and PU.1 in the propensity of B cells to undergo class-switch recombination (CSR) and ASC differentiation by concurrently promoting the expression of Bcl6 and Pax5 and repressing AID and Blimp1 (Carotta et al., 2014; Willis et al., 2017). Furthermore, cytokines secreted by T helper cells are known to play important roles in controlling B cell fate *in vivo*. Thus, additional regulatory interactions not represented in the current model, including IL-2-mediated activation of Bcl6 (through Stat5), IL-21-mediated activation of Blimp1 (through

Stat3), and IL-4-mediated activation of AID (Méndez and Mendoza, 2016; Moens and Tangye, 2014), are most likely necessary to account for *in vivo* differentiation.

The dynamics of cRel are regulated transcriptionally and through dimerization, sequestration by IκB inhibitors (Almaden et al., 2014; Alves et al., 2014; O'Dea and Hoffmann, 2009), and kinase activity (Shinohara et al., 2014). This motivated us to incorporate the NFκB-extended ASC model v2 into an established multi-scale B cell model (Mitchell et al., 2018; Shokhirev et al., 2015) that explicitly articulates these regulatory mechanisms. With single-cell resolution, the model recapitulated dynamical changes in cRel and Blimp1 expression, cellular proliferation, and subsequent differentiation of a subset of cells as measured by flow cytometry. Interestingly, the model also recapitulated the progression of PBs that have substantial proliferative capacity and are generated early in the immune response into terminally differentiated PCs that are quiescent and are generated late in the immune response. Thus, the multi-scale model can recapitulate the generation of heterogeneous ASC populations; however, further sources of heterogeneity, including the splenic architecture's role in extrafollicular PB and GC-derived PC generation, most likely remain to be investigated experimentally and incorporated into mathematical representations.

The resulting multi-scale model was also capable of recapitulating and disentangling altered proliferation and differentiation phases in systems with genetic perturbations in key regulators such as cRel, RelA, and Blimp1. Thus, the model represents an *in silico* laboratory that might be used iteratively with wet-lab experiments for mechanistically investigating the variety of B cell lymphomas subtypes. Our multi-scale modeling work, supported by quantitative experimental data, suggests that coordinated dynamic regulation of cRel and RelA is critical for the switch from proliferative to ASC differentiation phases, and perturbations within this network are associated with B cell malignancies. Consequently, we suggest that dynamic mis-coordination of cRel and RelA might be a more useful concept than hyper- or hypo-activity of generic NFκB when addressing the mechanisms underlying B cell lymphoma or humoral response deficiencies.

## STAR★METHODS

Detailed methods are provided in the online version of this paper and include the following:

- KEY RESOURCES TABLE
- CONTACT FOR REAGENT AND RESOURCE SHARING
- EXPERIMENTAL MODEL AND SUBJECT DETAILS
  - ○ Mice
  - ○ Cell Lines
- METHOD DETAILS
  - ○ B cell isolation and culture
  - ○ Sorting of B cells subtypes by flow cytometry
  - ○ Mouse immunization
  - ○ Isolation and characterization of intestinal ASC
  - ○ Genetic modification of BCL1 cells
  - ○ RNA and Immunoblot Analysis
  - ○ IgM production measurement by ELISA

- ○ Chromatin Immunoprecipitation (ChIP)
- ○ Measurement of apoptotic cells in ABC and LPS-PB
- ○ Measurement of generation-specific ASC
- ○ Intracellular staining
- ○ Cell Cycle Analysis
- ○ Computational Modeling of the ABC-ASC Differentiation Circuit
- ○ Multiscale Modeling
- QUANTIFICATION AND STATISTICAL ANALYSIS
- DATA AND SOFTWARE AVAILABILITY

### REFERENCES

Almaden, J.V., Tsui, R., Liu, Y.C., Birnbaum, H., Shokhirev, M.N., Ngo, K.A., Davis-Turak, J.C., Otero, D., Basak, S., Rickert, R.C., and Hoffmann, A. (2014). A pathway switch directs BAFF signaling to distinct NFκB transcription factors in maturing and proliferating B cells. Cell Rep. *9*, 2098–2111.

Alves, B.N., Tsui, R., Almaden, J., Shokhirev, M.N., Davis-Turak, J., Fujimoto, J., Birnbaum, H., Ponomarenko, J., and Hoffmann, A. (2014). IκBε is a key regulator of B cell expansion by providing negative feedback on cRel and RelA in a stimulus-specific manner. J. Immunol. *192*, 3121–3132.

Arjunaraja, S., Nosé, B.D., Sukumar, G., Lott, N.M., Dalgard, C.L., and Snow, A.L. (2017). Intrinsic plasma cell differentiation defects in B cell expansion with NF-κB and T cell anergy patient B cells. Front. Immunol. *8*, 913.

Calado, D.P., Zhang, B., Srinivasan, L., Sasaki, Y., Seagal, J., Unitt, C., Rodig, S., Kutok, J., Tarakhovsky, A., Schmidt-Supprian, M., and Rajewsky, K. (2010). Constitutive canonical NF-κB activation cooperates with disruption of BLIMP1 in the pathogenesis of activated B cell-like diffuse large cell lymphoma. Cancer Cell *18*, 580–589.

Carotta, S., Willis, S.N., Hasbold, J., Inouye, M., Pang, S.H.M., Emslie, D., Light, A., Chopin, M., Shi, W., Wang, H., et al. (2014). The transcription factors

IRF8 and PU.1 negatively regulate plasma cell differentiation. J. Exp. Med. *211*, 2169–2181.

Cattoretti, G., Angelin-Duclos, C., Shaknovich, R., Zhou, H., Wang, D., and Alobeid, B. (2005). PRDM1/Blimp-1 is expressed in human B-lymphocytes committed to the plasma cell lineage. J. Pathol. *206*, 76–86.

Ceribelli, M., Kelly, P.N., Shaffer, A.L., Wright, G.W., Xiao, W., Yang, Y., Mathews Griner, L.A., Guha, R., Shinn, P., Keller, J.M., et al. (2014). Blockade of oncogenic IκB kinase activity in diffuse large B-cell lymphoma by bromodomain and extraterminal domain protein inhibitors. Proc. Natl. Acad. Sci. USA *111*, 11365–11370.

Couter, C.J., Surana, N.K. (2016). Isolation and Flow Cytometric Characterization of Murine Small Intestinal Lymphocytes. J. Vis. Exp. 2016 May 8;(111). https://doi.org/10.3791/54114.

Davis, R.E., Brown, K.D., Siebenlist, U., and Staudt, L.M. (2001). Constitutive nuclear factor kappaB activity is required for survival of activated B cell-like diffuse large B cell lymphoma cells. J. Exp. Med. *194*, 1861–1874.

Di Niro, R., Lee, S.J., Vander Heiden, J.A., Elsner, R.A., Trivedi, N., Bannock, J.M., Gupta, N.T., Kleinstein, S.H., Vigneault, F., Gilbert, T.J., et al. (2015). Salmonella infection drives promiscuous B cell activation followed by extrafollicular affinity maturation. Immunity *43*, 120–131.

Duyao, M.P., Buckler, A.J., and Sonenshein, G.E. (1990). Interaction of an NF-kappa B-like factor with a site upstream of the c-myc promoter. Proc. Natl. Acad. Sci. USA *87*, 4727–4731.

Fujita, N., Jaye, D.L., Geigerman, C., Akyildiz, A., Mooney, M.R., Boss, J.M., and Wade, P.A. (2004). MTA3 and the Mi-2/NuRD complex regulate cell fate during B lymphocyte differentiation. Cell *119*, 75–86.

Grumont, R.J., and Gerondakis, S. (2000). Rel induces interferon regulatory factor 4 (IRF-4) expression in lymphocytes: modulation of interferon-regulated gene expression by rel/nuclear factor kappaB. J. Exp. Med. *191*, 1281–1292.

Hasbold, J., Corcoran, L.M., Tarlinton, D.M., Tangye, S.G., and Hodgkin, P.D. (2004). Evidence from the generation of immunoglobulin G-secreting cells that stochastic mechanisms regulate lymphocyte differentiation. Nat. Immunol. *5*, 55–63.

Heinzel, S., Binh Giang, T., Kan, A., Marchingo, J.M., Lye, B.K., Corcoran, L.M., and Hodgkin, P.D. (2017). A Myc-dependent division timer complements a cell-death timer to regulate T cell and B cell responses. Nat. Immunol. *18*, 96–103.

Heise, N., De Silva, N.S., Silva, K., Carette, A., Simonetti, G., Pasparakis, M., and Klein, U. (2014). Germinal center B cell maintenance and differentiation are controlled by distinct NF-κB transcription factor subunits. J. Exp. Med. *211*, 2103–2118.

Hoffmann, A., and Baltimore, D. (2006). Circuitry of nuclear factor kappaB signaling. Immunol. Rev. *210*, 171–186.

Hoffmann, A., Leung, T.H., and Baltimore, D. (2003). Genetic analysis of NF-kappaB/Rel transcription factors defines functional specificities. EMBO J. *22*, 5530–5539.

Hunter, J.E., Butterworth, J.A., Zhao, B., Sellier, H., Campbell, K.J., Thomas, H.D., Bacon, C.M., Cockell, S.J., Gewurz, B.E., and Perkins, N.D. (2016). The NF-κB subunit c-Rel regulates Bach2 tumour suppressor expression in B-cell lymphoma. Oncogene *35*, 3476–3484.

Kaileh, M., and Sen, R. (2012). NF-κB function in B lymphocytes. Immunol. Rev. *246*, 254–271.

Kallies, A., Hasbold, J., Fairfax, K., Pridans, C., Emslie, D., McKenzie, B.S., Lew, A.M., Corcoran, L.M., Hodgkin, P.D., Tarlinton, D.M., and Nutt, S.L. (2007). Initiation of plasma-cell differentiation is independent of the transcription factor Blimp-1. Immunity *26*, 555–566.

Kaplan, D., and Glass, L. (2012). Understanding nonlinear dynamics (Springer Science & Business Media).

Kim, Y., and Tian, M. (2009). NF-kappaB family of transcription factor facilitates gene conversion in chicken B cells. Mol. Immunol. *46*, 3283–3291.

Köntgen, F., Grumont, R.J., Strasser, A., Metcalf, D., Li, R., Tarlinton, D., and Gerondakis, S. (1995). Mice lacking the c-rel proto-oncogene exhibit defects in lymphocyte proliferation, humoral immunity, and interleukin-2 expression. Genes Dev. *9*, 1965–1977.

Landsverk, O.J., Snir, O., Casado, R.B., Richter, L., Mold, J.E., Réu, P., Horneland, R., Paulsen, V., Yaqub, S., Aandahl, E.M., et al. (2017). Antibody-secreting plasma cells persist for decades in human intestine. J. Exp. Med. *214*, 309–317.

Lin, Y., Wong, K., and Calame, K. (1997). Repression of c-myc transcription by Blimp-1, an inducer of terminal B cell differentiation. Science *276*, 596–599.

Lin, K.I., Lin, Y., and Calame, K. (2000). Repression of c-myc is necessary but not sufficient for terminal differentiation of B lymphocytes in vitro. Mol. Cell. Biol. *20*, 8684–8695.

Mandelbaum, J., Bhagat, G., Tang, H., Mo, T., Brahmachary, M., Shen, Q., Chadburn, A., Rajewsky, K., Tarakhovsky, A., Pasqualucci, L., and Dalla-Favera, R. (2010). BLIMP1 is a tumor suppressor gene frequently disrupted in activated B cell-like diffuse large B cell lymphoma. Cancer Cell *18*, 568–579.

Martínez, M.R., Corradin, A., Klein, U., Álvarez, M.J., Toffolo, G.M., di Camillo, B., Califano, A., and Stolovitzky, G.A. (2012). Quantitative modeling of the terminal differentiation of B cells and mechanisms of lymphomagenesis. Proc. Natl. Acad. Sci. USA *109*, 2672–2677.

Méndez, A., and Mendoza, L. (2016). A network model to describe the terminal differentiation of B cells. PLoS Comput. Biol. *12*, e1004696.

Minnich, M., Tagoh, H., Bönelt, P., Axelsson, E., Fischer, M., Cebolla, B., Tarakhovsky, A., Nutt, S.L., Jaritz, M., and Busslinger, M. (2016). Multifunctional role of the transcription factor Blimp-1 in coordinating plasma cell differentiation. Nat. Immunol. *17*, 331–343.

Mitchell, S., Roy, K., Zangle, T.A., and Hoffmann, A. (2018). Nongenetic origins of cell-to-cell variability in B lymphocyte proliferation. Proc. Natl. Acad. Sci. USA *115*, E2888–E2897.

Moens, L., and Tangye, S.G. (2014). Cytokine-mediated regulation of plasma cell generation: IL-21 takes center stage. Front. Immunol. *5*, 65.

Morgan, M.A.J., Magnusdottir, E., Kuo, T.C., Tunyaplin, C., Harper, J., Arnold, S.J., Calame, K., Robertson, E.J., and Bikoff, E.K. (2009). Blimp-1/Prdm1 alternative promoter usage during mouse development and plasma cell differentiation. Mol. Cell. Biol. *29*, 5813–5827.

Muto, A., Ochiai, K., Kimura, Y., Itoh-Nakadai, A., Calame, K.L., Ikebe, D., Tashiro, S., and Igarashi, K. (2010). Bach2 represses plasma cell gene regulatory network in B cells to promote antibody class switch. EMBO J. *29*, 4048–4061.

Nutt, S.L., Hodgkin, P.D., Tarlinton, D.M., and Corcoran, L.M. (2015). The generation of antibody-secreting plasma cells. Nat. Rev. Immunol. *15*, 160–171.

O'Dea, E., and Hoffmann, A. (2009). NF-κB signaling. Wiley Interdisc. Rev. Syst. Biol. Med. *1*, 107–115.

Park, S.R., Zan, H., Pal, Z., Zhang, J., Al-Qahtani, A., Pone, E.J., Xu, Z., Mai, T., and Casali, P. (2009). HoxC4 binds to the promoter of the cytidine deaminase AID gene to induce AID expression, class-switch DNA recombination and somatic hypermutation. Nat. Immunol. *10*, 540–550.

Pohl, T., Gugasyan, R., Grumont, R.J., Strasser, A., Metcalf, D., Tarlinton, D., Sha, W., Baltimore, D., and Gerondakis, S. (2002). The combined absence of NF-kappa B1 and c-Rel reveals that overlapping roles for these transcription factors in the B cell lineage are restricted to the activation and function of mature cells. Proc. Natl. Acad. Sci. USA *99*, 4514–4519.

Rosenwald, A., Wright, G., Chan, W.C., Connors, J.M., Campo, E., Fisher, R.I., Gascoyne, R.D., Muller-Hermelink, H.K., Smeland, E.B., Giltnane, J.M., et al.; Lymphoma/Leukemia Molecular Profiling Project (2002). The use of molecular profiling to predict survival after chemotherapy for diffuse large-B-cell lymphoma. N. Engl. J. Med. *346*, 1937–1947.

Saito, M., Gao, J., Basso, K., Kitagawa, Y., Smith, P.M., Bhagat, G., Pernis, A., Pasqualucci, L., and Dalla-Favera, R. (2007). A signaling pathway mediating downregulation of BCL6 in germinal center B cells is blocked by BCL6 gene alterations in B cell lymphoma. Cancer Cell *12*, 280–292.

Sciammas, R., and Davis, M.M. (2004). Modular nature of Blimp-1 in the regulation of gene expression during B cell maturation. J. Immunol. *172*, 5427–5440.

Sciammas, R., Li, Y., Warmflash, A., Song, Y., Dinner, A.R., and Singh, H. (2011). An incoherent regulatory network architecture that orchestrates B cell diversification in response to antigen signaling. Mol. Syst. Biol. *7*, 495.

Shaffer, A.L., Lin, K.I., Kuo, T.C., Yu, X., Hurt, E.M., Rosenwald, A., Giltnane, J.M., Yang, L., Zhao, H., Calame, K., and Staudt, L.M. (2002a). Blimp-1 orchestrates plasma cell differentiation by extinguishing the mature B cell gene expression program. Immunity 17, 51–62.

Shaffer, A.L., Rosenwald, A., and Staudt, L.M. (2002b). Lymphoid malignancies: the dark side of B-cell differentiation. Nat. Rev. Immunol. 2, 920–932.

Shapiro-Shelef, M., and Calame, K. (2005). Regulation of plasma-cell development. Nat. Rev. Immunol. 5, 230–242.

Shi, W., Liao, Y., Willis, S.N., Taubenheim, N., Inouye, M., Tarlinton, D.M., Smyth, G.K., Hodgkin, P.D., Nutt, S.L., and Corcoran, L.M. (2015). Transcriptional profiling of mouse B cell terminal differentiation defines a signature for antibody-secreting plasma cells. Nat. Immunol. 16, 663–673.

Shinohara, H., Behar, M., Inoue, K., Hiroshima, M., Yasuda, T., Nagashima, T., Kimura, S., Sanjo, H., Maeda, S., Yumoto, N., et al. (2014). Positive feedback within a kinase signaling complex functions as a switch mechanism for NF-κB activation. Science 344, 760–764.

Shokhirev, M.N., Almaden, J., Davis-Turak, J., Birnbaum, H.A., Russell, T.M., Vargas, J.A., and Hoffmann, A. (2015). A multi-scale approach reveals that NF-κB cRel enforces a B-cell decision to divide. Mol. Syst. Biol. 11, 783.

Staudt, L.M. (2010). Oncogenic activation of NF-kappaB. Cold Spring Harb. Perspect. Biol. 2, a000109.

Tarlinton, D., Radbruch, A., Hiepe, F., and Dörner, T. (2008). Plasma cell differentiation and survival. Curr. Opin. Immunol. 20, 162–169.

Tellier, J., Shi, W., Minnich, M., Liao, Y., Crawford, S., Smyth, G.K., Kallies, A., Busslinger, M., and Nutt, S.L. (2016). Blimp-1 controls plasma cell function through the regulation of immunoglobulin secretion and the unfolded protein response. Nat. Immunol. 17, 323–330.

Wang, L., Walker, B.L., Iannaccone, S., Bhatt, D., Kennedy, P.J., and Tse, W.T. (2009). Bistable switches control memory and plasticity in cellular differentiation. Proc. Natl. Acad. Sci. USA 106, 6638–6643.

Willis, S.N., Tellier, J., Liao, Y., Trezise, S., Light, A., O'Donnell, K., Garrett-Sinha, L.A., Shi, W., Tarlinton, D.M., and Nutt, S.L. (2017). Environmental sensing by mature B cells is controlled by the transcription factors PU.1 and SpiB. Nat. Commun. 8, 1426.

Xia, Y., Xu-Monette, Z.Y., Tzankov, A., Li, X., Manyam, G.C., Murty, V., Bhagat, G., Zhang, S., Pasqualucci, L., Visco, C., et al. (2017). Loss of PRDM1/BLIMP-1 function contributes to poor prognosis of activated B-cell-like diffuse large B-cell lymphoma. Leukemia 31, 625–636.

Yoon, H., and Boss, J.M. (2010). PU.1 binds to a distal regulatory element that is necessary for B cell-specific expression of CIITA. J. Immunol. 184, 5018–5028.

Yu, J., Angelin-Duclos, C., Greenwood, J., Liao, J., and Calame, K. (2000). Transcriptional repression by blimp-1 (PRDI-BF1) involves recruitment of histone deacetylase. Mol. Cell. Biol. 20, 2592–2603.

# STAR★METHODS

## KEY RESOURCES TABLE

| REAGENT or RESOURCE | SOURCE | IDENTIFIER |
|---|---|---|
| **Antibodies** | | |
| Rat Monoclonal anti-mouse CD16/32 (Fc receptor blocker) | BioLegend | Cat#101302; RRID: AB_312801 |
| Rat monoclonal anti-B220-eF450 | eBioscience | Cat#48-0452-82; RRID: AB_1548761 |
| Rat monoclonal anti-human/mouse B220-PE | eBioscience | Cat#12-0452-83; RRID: AB_465671 |
| Rat monoclonal anti-mouse/human B220-FITC | BioLegend | Cat#103206; RRID: AB_312991 |
| Rat monoclonal anti-mouse/human B220-APC-Cy7 | BioLegend | Cat#103223; RRID: AB_313006 |
| Armenian hamster monoclonal anti-mouse CD3e-FITC | eBioscience | Cat#11-0031-82; RRID: AB_469315 |
| Rat monoclonal anti-mouse CD11b-FITC | eBioscience | Cat#11-0112-82; RRID: AB_464935 |
| Rat monoclonal anti-mouse Ly-6C-Alexa 488 | eBioscience | Cat#53-5932-82; RRID: AB_2574427 |
| Armenian hamster monoclonal anti-mouse CD11c-FITC | eBioscience | Cat#11-0114-82; RRID: AB_464940 |
| Rat monoclonal anti-mouse CD49b-FITC | eBioscience | Cat#11-5971-82; RRID: AB_465327 |
| Mouse monoclonal anti-mouse FAS-APC | BioLegend | Cat#152604; RRID: AB_2632899 |
| Rat monoclonal anti-mouse CD38-PE | BioLegend | Cat#102708; RRID: AB_312929 |
| Rat monoclonal anti-mouse CD138-PE | BioLegend | Cat#142504; RRID: AB_10916119 |
| Rat monoclonal anti-mouse CD138-PerCP Cy5.5 | BioLegend | Cat#142509; RRID: AB_2561600 |
| Rat monoclonal anti-mouse CD138-APC | BioLegend | Cat#142506; RRID: AB_10962911 |
| Rat monoclonal anti-mouse CD138-Biotin | BioLegend | Cat#142511; RRID: AB_2561980 |
| Rat monoclonal anti-mouse Ly-6G-FITC | BioLegend | Cat#127605; RRID: AB_1236488 |
| Rat monoclonal anti-mouse Blimp1-Alexa 647 | BioLegend | Cat#150003; RRID: AB_2565617 |
| Rat monoclonal anti-mouse cRel- PE | eBioscience | Cat#12-6111-80; RRID: AB_11042978 |
| Rat monoclonal anti-mouse cRel-eF660 | eBioscience | Cat#50-6111-80; RRID: AB_2574260 |
| Mouse monoclonal anti-Rela-PE | Cell Signaling | Cat#9460 |
| Rabbit polyclonal anti-Rela | SantaCruz | Cat#sc-372: RRID: AB_632037 |
| Rabbit polyclonal anti-cRel | SantaCruz | Cat#sc-71; RRID: AB_2253705 |
| Rat monoclonal anti-Blimp1 | SantaCruz | Cat#sc-47732; RRID: AB_628168 |
| Goat polyclonal anti-IRF4 | SantaCruz | Cat#sc-6059; RRID: AB_2127145 |
| Rabbit polyclonal anti-Bach2 | Abcam | Cat#ab83364; RRID: AB_1861444 |
| Goat polyclonal anti-Actin | SantaCruz | Cat#sc-1615; RRID: AB_630835 |
| Rabbit polyclonal Anti-Histone H3 (acetyl K9) | Abcam | Cat#ab4441; RRID: AB_2118292 |
| Rabbit isotype IgG | SantaCruz | Cat#sc-2027; RRID; AB_737197 |
| **Chemicals, Peptides, and Recombinant Proteins** | | |
| fixable viability dye eF506 | Affymetrix Bioscience | Cat#65-0866-18 |
| 7 aminoacitomycine D (7AAD) | BioLegend | Cat#420404 |
| **Critical Commercial Assays** | | |
| Ig isotyping ELISA kit | eBioscience | Cat#88-50630-88 |
| Dead Cell Apoptosis Kit | ThermoFisher Scientific | Cat# V13241 |
| CellTrace™ Far Red Cell Proliferation Kit | ThermoFisher Scientific | Cat#C34564 |
| Fix and Perm cell permeabilization kit | ThermoFisher Scientific | Cat#GAS003 |
| **Experimental Models: Cell Lines** | | |
| HEK293T | ATCC | CRL-3216: RRID: CVCL_0063 |
| BCL1 | ATCC | CRL-1669: RRID: CVCL_4120 |
| **Experimental Models: Organisms/Strains** | | |
| Mouse: C57BL/6 | The Jackson Laboratory | JAX: 000664; RRID: IMSR_JAX:000664 |
| Mouse: C57BL/6: $rel^{-/-}$ | Köntgen et al., 1995 | N/A |

*(Continued on next page)*

*Continued*

| REAGENT or RESOURCE | SOURCE | IDENTIFIER |
|---|---|---|
| Oligonucleotides | | |
| pLX-cRel, Bach2 KO guide RNA (5′-CACCGGAACTTTCGTCC CCCTGCGC-3′, 5′-CACCGTGCTGCAGGGACGGGCACAA-3′) | This paper | N/A |
| Blimp1 KO guide RNA (5′-CACCGGAATCCAGCTCACTCTG CCC-3′, 5′-CACCGACCTGGCTGCCTGTCAGAAC −3′) | This paper | N/A |
| Blimp1 binding site disruption guide RNA (5′-CACCGTACTA GAGCATCTGAAAGCC-3′) | This paper | N/A |
| Blimp1 PCR primer: ACTTAAAGCCTTTTTGTGCTTCT and CAGTTTCCTTTACAGCAGGAGTT | This paper | N/A |
| Software and Algorithms | | |
| Graphpad Prism | GraphPad Software | N/A; RRID: SCR_001622 |
| Mathworks MATLAB | MathWorks, Inc | R2014a |
| Other | | |
| All Computational Modeling Code | This paper | http://www.signalingsystems.ucla.edu/ models-and-code/ |

## CONTACT FOR REAGENT AND RESOURCE SHARING

Further information and requests for resources and reagents should be directed to and will be fulfilled by the Lead Contact, Alexander Hoffmann (ahoffmann@ucla.edu).

## EXPERIMENTAL MODEL AND SUBJECT DETAILS

### Mice

Mice were maintained in environmental control facilities at the University of California, Los Angeles. Mice of both sexes were littermates and were 10-14 weeks old unless otherwise indicated. The $Rel^{-/-}$ (protein name cRel) mice (Köntgen et al., 1995) previously described and wild-type mice were in C57BL/6 genetic background. Animal work was performed according to University of California, Los Angeles regulations under an approved protocol.

### Cell Lines

HEK293 (ATCC, CRL-1573) cells were cultured with DMEM, 10% FBS. BCL1 (ATCC, CRL-1669) were cultured with RPMI, 10% FBS, 5 mM L-glutamine, and 55 μM 2-Mercaptoethanol.

## METHOD DETAILS

### B cell isolation and culture

Spleens were harvested from 10-12 weeks old female C57BL/6 mice and $Rel^{-/-}$ mice. Homogenized splenocytes were incubated with anti-CD43 magnetic beads for 15 min at 4-8°C, washed with MACS buffer (Phosphate buffer saline, (pH 7.4), 0.5% bovine serum albumin and 2 mM Ethylenediaminetetraacetic acid (pH 8)) and passed through LS column (Miltenyi Biotech). The purity of B cells was > 95% based on B220 staining as described previously (Mitchell et al., 2018). Briefly, the enriched B cell population was stained with B220-eF450, CD3e-FITC, CD11b-FITC and Ly-6C-Alexa 488. The stained cells were gated on B220$^+$CD3e$^-$CD11b$^-$Ly-6C$^-$.

B cells were grown in fresh media with 1% penicillin streptomycin solution, 5 mM L-glutamine, 20 mM HEPES buffer, 1mM MEM non-essential amino acid, 1 mM Sodium pyruvate, 10% FBS, and 55 μM 2-Mercaptoethanol.

### Sorting of B cells subtypes by flow cytometry

Mature splenic B cells were plated in a 10 cm Petri-dish and treated with LPS (10 μg/mL) for 72 h in 10 mL media with 1x10$^6$ cells/mL. Cells were harvested and resuspended in 100 μL of cold media. Nonspecific binding was blocked with Fc receptor blocker by incubating for 10 min on ice and stained with B220-eF450 and CD138-APC in a total of 200 μL of cold media for 30 min in ice. The excess antibody was removed and washed by centrifugation at 500 rcf, 4°C for 3 min, and then tubes were turned 180° and centrifugation was repeated. Cells were resuspended in media and dead cells were excluded using 7AAD. ABCs (B220$^{hi}$CD138$^-$) and ASCs (B220$^{low}$CD138$^+$) were sorted based on expression of B220 and CD138 by flow cytometer (Figure S2A).

Inguinal lymph nodes were isolated from immunized mice. GC B cells were sorted at 7 days after primary immunization. Homogenized lymph nodes were incubated with Fc receptor blocker for 10 min in ice and stained with B220-eF450, CD3e-FITC, CD11b-FITC, CD11c-FITC, CD49b-FITC, FAS-APC and CD38-PE in a total of 100 μL of cold media for 30 min in ice. GC B cell were sorted

using the gating strategy B220$^+$CD38$^-$FAS$^+$ (Figure S2F). ASCs were isolated from lymph nodes 7 days after a booster dose of immunization. Homogenized lymph nodes were incubated with Fc receptor blocker for 10 min in ice and stained with B220-eF450, CD3e-FITC, CD11b-FITC, CD11c-FITC, CD49b-FITC and CD138-APC in total 100 μL of cold media for 30 min in ice. ASCs were sorted using gating strategy B220$^{low}$CD138$^+$ (Figure S2G).

## Mouse immunization

10-12 weeks old female C57BL/6 mice were immunized with 100 μg of NP-OVA emulsified in Complete Freund Adjuvant in the foot pad, followed by an equivalent booster shot after 21 days.

## Isolation and characterization of intestinal ASC

Isolation of murine lymphocytes from the small-intestinal lamina propria was performed as previously described (Couter and Surana, 2016). Briefly, resected small-intestinal segments were washed, inverted, and the epithelial fraction was removed by incubating for 15 min at 37°C in RPMI with 5 mM DTT, 1 mM EDTA, and 2% FBS. The residual fraction was minced and digested for 30 min at 37°C in RPMI with collagenase II (1.5 mg/mL), dispase (0.5 mg/mL), and 1% FBS. Lamina propria single-cell suspensions were obtained by passing through 100 uM and 40 uM cell strainers, and resuspended in RPMI containing 2% FBS. Homogenized cells were incubated with fixable viability dye eF506 (Affymetrix Bioscience, #65-0866-18) in total 1 mL PBS for 30 min on ice and washed with PBS. Cells were then incubated with Fc receptor blocker for 10 min in ice and stained with B220-APC-Cy7, CD3e-FITC, CD11b-FITC, CD11c-FITC, CD49b-FITC, Ly-6G-FITC and CD138-PerCP Cy5.5 in total 100 μL of cold media for 30 min in ice. The gating strategy is similar to lymph node ASCs. B cells and ASCs were characterized using B220$^+$ and B220$^-$CD138+ respectively.

## Genetic modification of BCL1 cells

To lentivirally transduce BCL1 cells, HEK293 cells were transfected with all lentivirus constructs using lipofectamine (Invitrogen). 48 h post transfection, virus was harvested and used to infect murine BCL1 cells in the presence of polybrene (7.5 μg/mL). Lentivirally infected BCL1 cells were grown in the presence of puromycin for 3 days (Yoon and Boss, 2010). Plasmids used: pLX-cRel, *Bach2*$^{-/-}$ guide RNA (5′-CACCGGAACTTTCGTCCCCCTGCGC-3′ and 5′-CACCGTGCTGCAGGGACGGGCACAA-3′) and *Blimp1*$^{-/-}$ guide RNA (5′-CACCGGAATCCAGCTCACTCTGCCC-3′ and 5′-CACCGACCTGGCTGCCTGTCAGAAC −3′) cloned in the LentiV2 plasmid. The efficiency of knock in and knock out was assessed by immunoblot as indicated.

Electroporation of BCL1 cells was performed as described previously (Lin et al., 2000; Lin et al., 1997) with some modifications. Briefly, 2 x10$^5$ cells were plated and washed with PBS (without Ca2$^+$ and Mg2$^+$). Cells were resuspended in Resuspension Buffer R at 2x10$^5$ cells/10 μL and 1 μg of plasmid DNA was added. Cells were gently pipetted to obtain a single cell suspension. Cells were electroporated in Neon Transfection systems (Invitrogen) and plated in 6 well plates. A pulse voltage of 1000 mW and width of 40 ms was used for electroporation. Electroporated cells were grown in the presence of puromycin for 3 days. Blimp1 binding site disruption (*Rel*$^{BBS}$) was performed using guide RNA (5′-CACCGTACTAGAGCATCTGAAAGCC-3′) cloned in the Lentiv2 plasmid. The efficiency of mutation was measured by Next Generation Sequencing. The targeted genomic region was PCR amplified (using the primer: ACTTAAAGCCTTTTTGTGCTTCT and CAGTTTCCTTTACAGCAGGAGTT) and PCR products were gel purified. The purified PCR products were submitted for amplicon-EZ (150-500 bp) sequencing (Genewiz). Adaptor-trimmed sequencing results were processed for quality control using FASTX-Toolkit. A Python script was then used to analyze counts of unique mutated or wild-type amplicons (code is available as Supplemental File 1). Piechart was plotted with Graphpad Prism (Figure S4C).

## RNA and Immunoblot Analysis

For qPCR, mRNA was isolated from B cells, ABCs, ASCs, 10 μg/mL LPS-stimulated wild-type and *Rel*$^{-/-}$ B cells following 24, 36, 38, 60 and 72 hours of culture and BCL1 cells following stimulation with IL-2 (20 ng/mL) and IL-5 (20 ng/mL), using the Zymo Research kit. 1 μg mRNA was used to prepare cDNA using Oligo (dT) and quantitation was performed using the SSO syber green. Expression was normalized using ubiquitin C as a housekeeping gene. The primers used in this study are specified in Table S3.

For Immunoblot analysis, whole-cell lysates were prepared using RIPA lysis buffer. The resulting lysates were run on either 10% SDS-PAGE gels or 5%–14% Criterion Tris-HCl Gel (Bio-Rad). The following antibodies were used to identify the protein of interest: Rela, cRel, Blimp1, IRF4, Bach2 and actin (all from Santa Cruz Biotechnology). The resulting proteins were detected using the Bio-Rad ChemiDoc XRS System and SuperSignal West Femto Substrate Maximum Sensitivity Substrate (Thermo Scientific) to detect chemiluminescence released by HRP-labeled secondary antibodies.

## IgM production measurement by ELISA

For ELISA analysis, BCL1 and genetically modified BCL1 cells were plated in a 48 well plate with 2x10$^5$ cells/well in a 250 μl volume. The cells were stimulated with IL-2 (20 ng/mL) and IL-5 (20 ng/mL) for 96 hr and the supernatant was collected. The resulting supernatant was tested to measure secreted IgM by ELISA. ELISA was performed using mouse Ig isotyping ELISA kit according to manufacturer protocol.

## Chromatin Immunoprecipitation (ChIP)

For ChIP experiments 10x10$^6$ cells were washed with 10 mL PBS at room temperature (RT) and fixed with freshly supplemented 1% methanol-free formaldehyde and incubated at RT for 10-15 min with gentle shaking. The fixation reaction was quenched with 500 mM

Tris pH 8 for 2-5 min. The cells were washed twice with cold PBS followed by snap freezing with dry ice. The cell pellets were thawed and resuspended on ice in 1 mL Lysis Buffer 1 and incubated on a nutator at 4°C for 10 min before centrifugation at 800 rcf, 5 min, 4°C; supernatant was then discarded. Similar steps were performed with 1 mL Lysis Buffer 2. The nuclei were resuspended in 0.5 mL Lysis Buffer 3 Plus and incubated on ice for 10 min. The lysates were transferred into 1.5 mL TPX tubes (Diagenode #C30010010-1000, min 100 μl-max 300 μl/tube) and sonicated with a Bioruptor water bath sonicator using 25 cycles consisting of 30 s ON/30 s OFF at low intensity, 4°C. Sonication was stopped every 5 cycles for incubation on ice for 1 min, gentle inversion and pulse-spin. Aliquots were consolidated with the same sample into a single 1.5 mL polypropelene tube. The lysate was centrifuged at max speed for 15 min at 4°C. The supernatants were transferred to 1.5 mL no-stick microtubes (Phenix Research #MH-815S) and 3 volumes of dilution buffer were added to lysates. Unconjugated beads (25 μl/mL of diluted lysate) were washed (twice with PBS and dilution buffer) and dried up in no-stick tubes using a magnet. Lysates were mixed with dry beads and incubated for 2 hr at 4°C on a nutator. Lysates were used for the next step and beads were discarded. 1% aliquots were taken as input and stored at 4°C with volumes noted. 2 μg anti-H3K9ac antibody and isotype IgG were incubated with the lysate overnight at 4°C on a nutator. 25 μl protein G-conjugated magnetic beads (Active Motif #53014) were washed twice with Dilution Buffer, then once with low-salt buffer. Beads were dried using a magnetic rack. Lysates were transferred to dry beads and incubated for 5 hr at 4°C on a nutator. Beads were collected using a magnetic stand and washed twice with each of the following ice-cold buffers in order: low salt, high salt, LiCl, TE. 600 μl of buffer was used in each wash step and beads were resuspended by inversion, and placed in a high-speed shaker at RT for 5 min. Beads were resuspended in 70 μl of 250 mM NaCl. Input fractions were recovered and volumes were adjusted to 70 μl with 250 mM final concentration of NaCl. Both input and IP fractions were processed in a similar way after this. 50 μg DNase-free RNase A (Roche #11119915001) was added and incubated at 37°C for 1 hr with gentle mixing. SDS was added for a 1% final concentration and then 50 μg Proteinase K (Roche # 03115828001) was added for an overnight incubation at 60°C with gentle shaking. SPRI beads were resuspended by gentle vortexing, allowed to warm to RT and the supernatant was removed from Protein G beads. Protein G beads were washed with an additional 30 μl of 500 mM NaCl and combined with the first eluate. 0.9-1.0 volumes of SPRI beads were added and incubated at RT for 15 min on a nutator. Beads were collected using a magnetic stand and supernatants were removed. Beads were twice washed with 80% ethanol and residual ethanol from tubes was removed by air-drying beads for 5 min. DNA was eluted from beads with 30 μl TE buffer. Enrichment of the targeted DNA in the elution was measured by qPCR and the enrichment was calculated with respect to input.

### *Buffer composition*

Lysis Buffer 1: 50 mM HEPES-KOH, pH 7.6, 140 mM NaCl, 1 mM EDTA, 10% Glycerol, 0.5% NP-40, 0.25% Triton X-100, EDTA-free protease inhibitors.

Lysis Buffer 2: 10 mM Tris-HCl, pH 8.0, 200 mM NaCl, 1 mM EDTA, 0.5 mM EGTA, EDTA-free protease inhibitors.

Lysis Buffer 3: 10 mM Tris-HCl, pH 8.0, 100 mM NaCl, 1 mM EDTA, 0.5 mM EGTA, 0.1% Na Deoxycholate, 0.5% N-lauroylsarcosine, sodium salt (Sigma-Aldrich #61739), EDTA-free protease inhibitors.

Dilution Buffer: 10 mM Tris-HCl, pH 8.0, 160 mM NaCl, 1 mM EDTA, 0.01% SDS, 1.2% Triton X-100, EDTA-free protease inhibitors.

Low Salt Wash Buffer: 50 mM HEPES-KOH, pH 7.6, 150 mM NaCl, 1 mM EDTA, 1% Triton X-100, 0.1% Na Deoxycholate, 0.1% SDS, EDTA-free protease inhibitors.

High Salt Wash Buffer: 50 mM HEPES-KOH, pH 7.6, 500 mM NaCl, 1 mM EDTA, 1% Triton X-100, 0.1% Na Deoxycholate, 0.1% SDS.

LiCl Buffer: 20 mM Tris-HCl, pH 8.0, 250 mM LiCl, 1 mM EDTA, 0.5% Na Deoxycholate, 0.5% NP-40.

TE Buffer (10 mM Tris-HCl, pH 7.5, 1 mM EDTA)

### Measurement of apoptotic cells in ABC and LPS-PB

WT and *Rel*$^{-/-}$ B cells were treated with LPS (10 μg/mL) for 72 h as described above. Cells were harvested and resuspended in 100 μL of cold media. Nonspecific binding was blocked with Fc receptor blocker by incubating for 10 min on ice and stained with B220-PE and CD138-APC in a total of 200 μL of cold media for 30 min in ice. Stained cells were washed with FACS buffer (PBS with 5% FBS) and resuspended in Annexin V binding buffer. The staining of Annexin V Alexa Fluor 488 and Propidium Iodide (PI) was performed using Dead Cell Apoptosis Kit (ThermoFisher Scientific, # V13241) as described by manufacturer protocol. Briefly, 5 μL Alexa Fluor 488 annexin V and 1 μL PI (100 μg/mL PI working solution) were added to 100 μL of cell suspension. The cells were incubated at room temperature for 15 min. 400 μL annexin-binding buffer was added, mixed gently, and the samples were acquired in BD LSRFortessa flow cytometry (BD Bioscience). Data were analyzed with FlowJo. The gating strategy and ABC and LPS-PBs were characterized by as described above. ABC and LPS-PBs population were gated for Annexin V and PI positivity. The apoptotic cells were defined as AnnexinV$^+$PI$^-$ (Figure S5C).

### Measurement of generation-specific ASC

WT and *Rel*$^{-/-}$ B cells stained with Cell Trace Far Red (CTR) using CellTrace Far Red Cell Proliferation Kit (ThermoFisher Scientific, # C34564) as described by the manufacturer protocol. Briefly, cells were resuspended in 1 mL RT PBS and incubated with 1 μL CTR for 25 min at RT with rotation. Cells were washed followed by resuspension in RPMI with 10% FBS and incubated for 10 min at RT. The cells were washed and washing steps were repeated 1 more time. CTR labeled cells were treated with LPS (10 μg/mL) for 24 h, 48 h, 72 h and 96 h as described above. The cells were harvested at indicated time points, stained for CD138 and 7AAD as described above. The cells were acquired in CytoFlex flow cytometer. Dead (7AAD$^+$) cells were exclude from the analysis and the data were

analyzed in FlowJo. Cell generation number was defined based on dilution of CTR and ASCs were defined by expression of CD138. The generation specific percentage of ASC were calculated using the equation:

$$\text{Proportion ASC in generation}(n) = \frac{Number\ of\ ASC\ in\ generation(n)}{Number\ of\ total\ cells\ in\ generation(n)}$$

For each generation, n.

### Intracellular staining

Naive mature B cells (B cells) were isolated from spleens as described above. Cells were treated with LPS (10 μg/mL) in 12 well plates (5x10$^5$/well) for 0, 24, 48, 72 and 96 hours. Cells were washed twice with PBS, followed by permeabilization and staining with primary antibody and then secondary antibody using Fix and Perm cell permeabilization kit (ThermoFisher, # GAS003). Cell permeabilization and staining protocol as described by the manufacturer was followed. Cells were stained with cRel-PE and Blimp1-Alexa 647 antibody to measure expression of cRel and Blimp1 respectively by flowcytometry.

B cells were treated with anti-CD40 antibody (10 μg/mL) and IL-4 (5 ng/mL) for 72 h and stained for ABCs and CD40-PB as described above. Intracellular expression of cRel and Rela was measured using cRel-eF660 and Rela-PE respectively by flowcytometry using CytoFlex flow cytometry (488nm 50mW laser) (Beckman Coulter) and data were analyzed with FlowJo.

Intestinal lymphocytes were isolated and characterized as described above. Intracellular expression of cRel and Blimp1 was measured using cRel-PE and Blimp1-Alexa 647 respectively by BD LSRFortessa flow cytometry (BD Bioscience) and data were analyzed with FlowJo.

### Cell Cycle Analysis

BCL1 and BCL1-cRel cells were plated in a 35 mm Petri-dish with 1x10$^6$ cells in a 2 mL volume. The cells were stimulated with IL-2 (20 ng/mL) and IL-5 (20 ng/mL) for 24 hr. The cells were harvested and washed with cold PBS. The cell pellets were fixed by drop wise addition of 70% cold ethanol with continuous mild vortex and cells were kept overnight (16-20 hr) at 4°C. The cells were washed with PBS twice by centrifugation 850 rcf for 5 min at 4°C and turned the tube 180° to repeat centrifugation. Cells were treated with 50 μl of a 100 μg/mL sock of RNase A for 15 min at 37°C and 200 μl of propidium iodide (PI) from 50 μg/mL stock solution were incubated for 15 min at RT.

The cells were acquired in flow cytometer (CytoFLEX, Beckman Coulter). The cells were gated based on forward scattered (FSC) and side scattered to identify single cells. Doublet were excluded from analysis using FSC area and FSC width. The DNA content was measured by staining with PI.

### Computational Modeling of the ABC-ASC Differentiation Circuit

Computational modeling was performed in MATLAB by re-constructing the system of ODEs, with identical parameters and reactions as described by Sciammas et al. (2011). ODE solver ODE45 was used throughout. To construct the NFκB-extended ASC model v1, cRel and RelA were included with two additional differential equations. Additional reactions were included as shown in Figures 1B and 3A with similar kinetic rate laws. Briefly, degradation was mass action with Hill equations used for activation and inhibition. Parameters and thresholds were chosen to be consistent with Sciammas et al. and maintained the same throughout (Sciammas et al., 2011). All equations, parameters and initial conditions are given in Data S1, Tables S1 and S2. While the previously published model sampled IRF4 activation rates to simulate cell-to-cell variability of activation strength, here we sampled cRel and Rela activation rates with the same coefficient of variation (0.4) as used for IRF4 in Sciammas et al.

cRel downregulation (Figure 1) was investigated by running a time course simulation of 125 individual cells for 96 hours then taking the final molecular abundances as an initial condition of a subsequent 96 hour simulation in which cRel expression was reduced as indicated.

To construct the NFκB-extended ASC model v2, Blimp1-mediated cRel downregulation was incorporated through hill kinetics consisted with the NFκB-extended ASC model model v1. Constant cRel expression ($e_c = 1$) was replaced with:

$$cRel_{exp} = e_c \cdot \left( \frac{K_r^{n_r}}{K_r^{n_r} + [BLIMP]^{n_r}} \right).$$

To simulate $Rel^{-/-}$ we set cRel expression to 0 and simulated a population of 125 individual cells. ASC generation in cRel deficiency is controlled by RelA, RT-PCR analysis showed that $Rel^{-/-}$ B cells reduced RelA expression at 24 h (20%–40%) and had very similar expression at 72 h compared to wild-type. This was incorporated into our $Rel^{-/-}$ simulations through reducing RelA expression rate (40% of WT) up to 24h and returning this rate to near WT (70% of WT) for the remaining simulation time.

### Multiscale Modeling

The NFκB-extended ASC model v2 constructed here was combined with a published model of B cell proliferation (Mitchell et al., 2018) to create a multiscale model capable of simulating the division, death and differentiation of a population of individual cells. All reactions and parameters within the differentiation circuit were maintained as described here and all reactions and parameters within the NFκB, apoptosis and mitosis networks were maintained as described by Mitchell et al. (Mitchell et al., 2018). NFκB

activation sampling as described above for NFκB-extended ASC model v1 and v2 was not performed here as cell-to-cell variability was quantified in Mitchell et al. and simulated here in the same manner resulting in realistically distributed NFκB activities. As the absolute concentration of cRel in the differentiation model and multiscale model differed (due to the arbitrary concentrations of molecular species in the previously published differentiation model (Sciammas et al., 2011)) the $K_D$ of cRel- and Rela-mediated reactions in the differentiation circuit were scaled to be approximately half the maximum cRel and Rela concentrations observed in simulations from Mitchell et al. A population of 1000 single cells was simulated and scatterplots of cRel versus Blimp1 were created every 15 min for 124 hours (Video S1 and Figure 6E). $Rel^{-/-}$ simulations were performed by removing cRel expression and reducing RelA expression as described for the ASC differentiation model. A similar approach was taken to Blimp1, with $Blimp1^{-/-}$ simulated by scaling Blimp1 expression by 50%. $Rel^{BS-seq}$ cells were simulated by removing terms representing Blimp1 inhibition of cRel expression from the ODE for cRel. cRel-High simulations were performed by increasing cRel expression 5-fold. All code is available at http://www.signalingsystems.ucla.edu/models-and-code/.

## QUANTIFICATION AND STATISTICAL ANALYSIS

Details of the statistical tests applied to replicates of datasets shown in Figures can be found in the corresponding Figure legends. Statistical analyses were performed using GraphPad Prism 7 software. $*p < 0.05$, $**p < 0.01$, $***p < 0.001$ and not significant (ns) (Unpaired Students t test).

## DATA AND SOFTWARE AVAILABILITY

Equations of the mathematical model of the ABC-ASC differentiation circuit are provided in Data S1. MATLAB code for all models is available at http://www.signalingsystems.ucla.edu/models-and-code/. The analysis tool of CRISPR mutation efficiency is available as python code as Data S2.

**Supplemental Information**

**A Regulatory Circuit Controlling**

**the Dynamics of NFκB cRel Transitions B Cells**

**from Proliferation to Plasma Cell Differentiation**

Koushik Roy, Simon Mitchell, Yi Liu, Sho Ohta, Yu-sheng Lin, Marie Oliver Metzig, Stephen L. Nutt, and Alexander Hoffmann
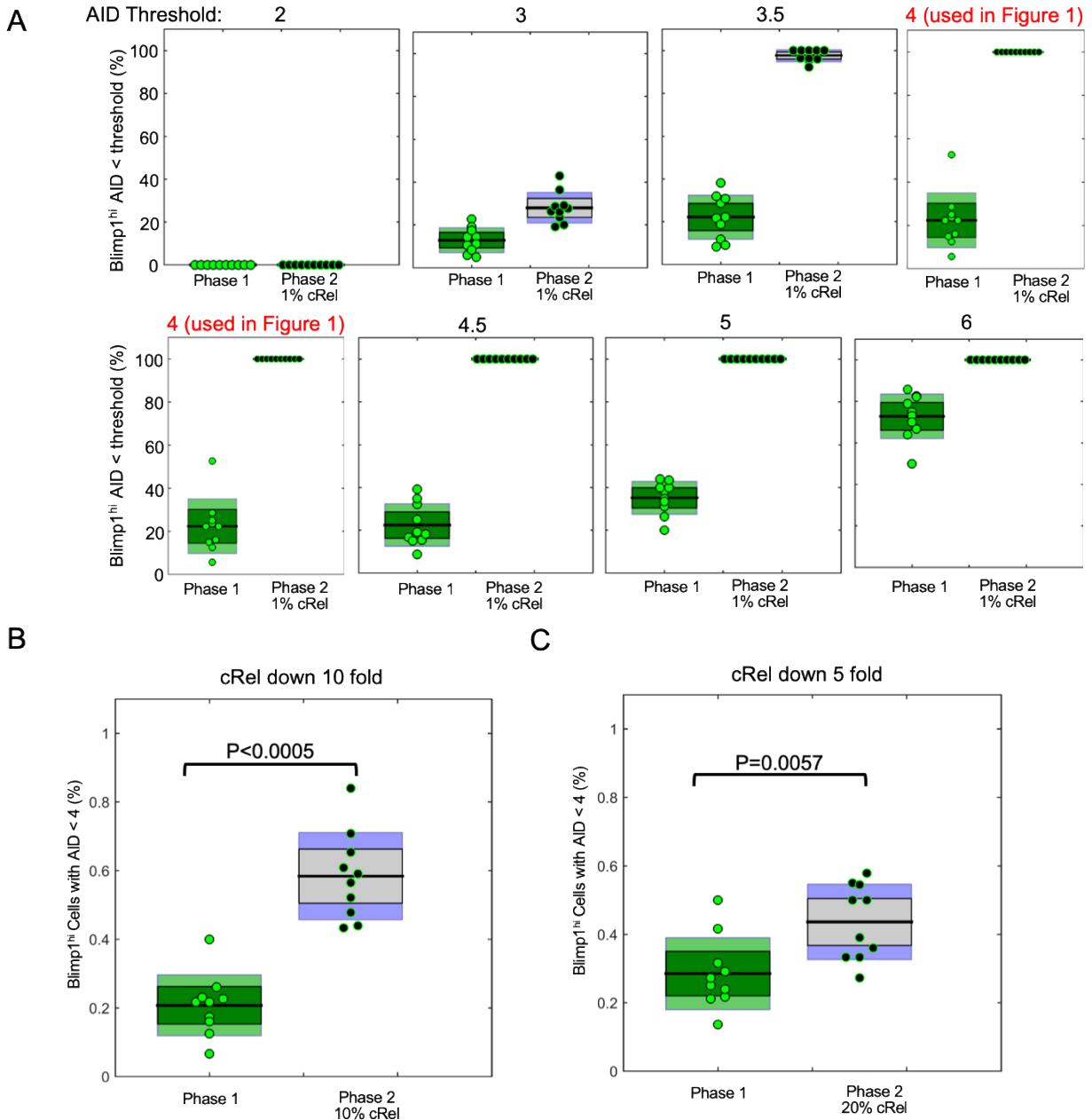
**Figure S1 (Related to Figure 1): cRel downregulation enables ASC production in simulations regardless of the AID threshold used to define an ASC. A)** Percentage of cells with Blimp1>4 and AID<4 (representing ASCs) after an initial (phase 1) simulation with the NFκB-extended model v1 and subsequent (phase 2) simulation in which cRel is reduced to 1%. Each point indicates the final ASC percentage in 125 cells after 96 hours. **B) and C)** Bar graph of ASC percentage generated in phase 2 simulations with 10 fold (left) and 5 fold (right) cRel downregulation respectively. Median (black), standard deviation (dark green) and standard error mean (light green) are indicated.
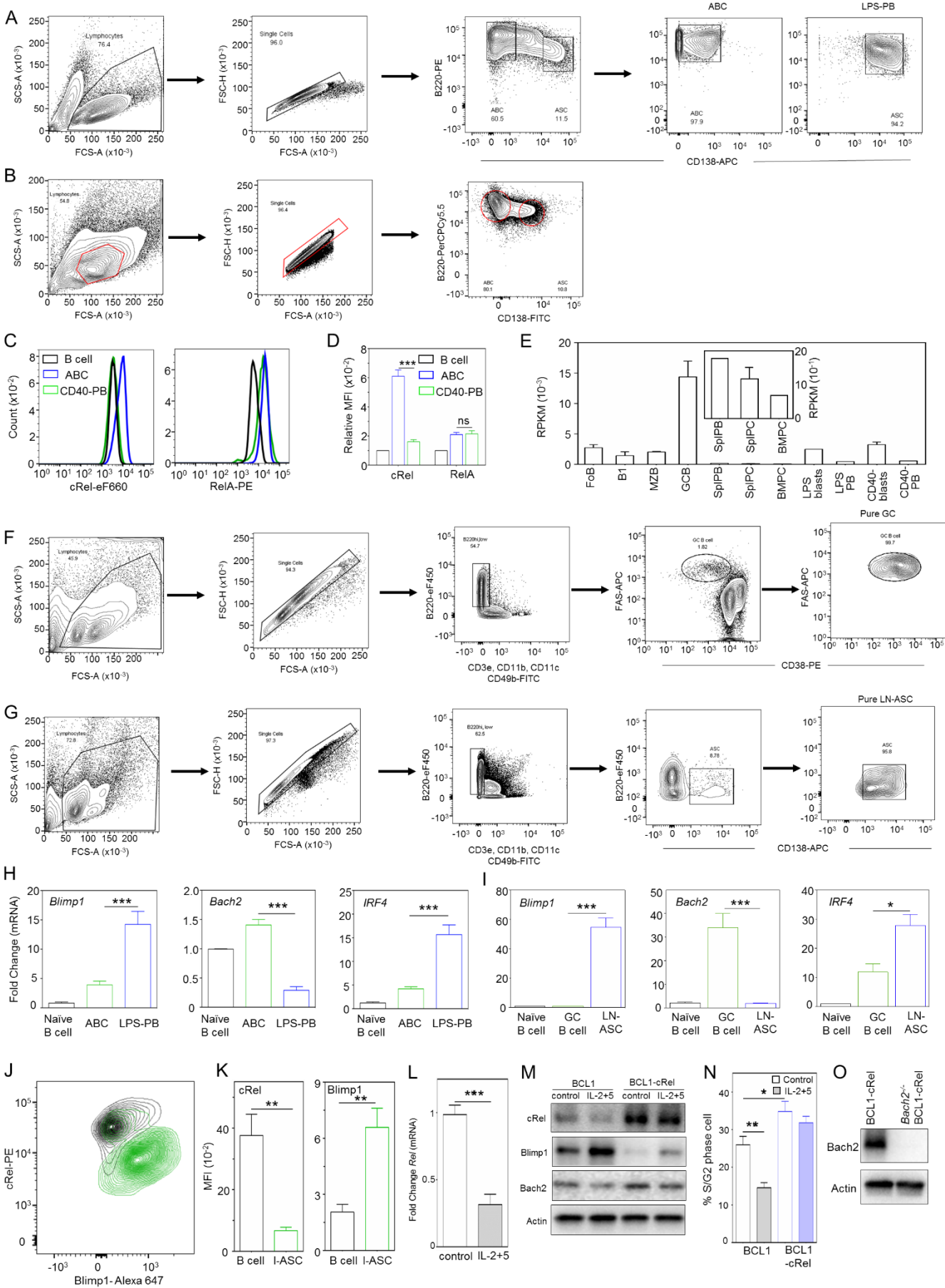
**Figure S2 (Related to Figure 2): Purification and confirmation of ABCs and ASCs with cRel expression. A)** Gating strategy and flow cytometry plot showing purity of e*x-vivo* generated ABCs and LPS-PBs upon stimulation with LPS. ABCs and LPS-PBs were determined by B220$^{low}$CD138$^{+}$ and B220$^{+}$CD138$^{-}$. Cell percentage of ABCs (60.5%) and LPS-PBs (11.5%). Purity of ABCs (97.9%) and LPS-PBs (94.2%). **B)** Gating strategy and flow cytometry plot of ABCs and CD40-PBs upon stimulation with anti-CD40 antibody and IL-4. **C)** Histograms of cRel (left) and RelA (right) expression in B cells (black), ABCs (blue) and plasmablast (green, CD40-PB) upon stimulation with anti-CD40 antibody and IL-4. cRel and RelA expression was measured by intracellular staining followed by flow cytometry and X-axis indicates the fluorescence intensity. **D)** Bar graph of relative mean fluorescence intensity (MFI) of cRel and RelA, relative to naïve B cells (1). **E)** Bar graph of *Rel* expression (RPKM) in Follicular B cells (FoB), B1 B cells (B1), Marginal Zone B cells (MZB), Germinal Center B cells (GCB), Splenic Plasmablasts (SplPB), Splenic Plasma Cells (SplPC), Bone Marrow Plasma Cells (BMPC), LPS stimulated B cells (LPS-B), Plasmablasts generated upon LPS stimulation (LPS-PB), CD40+ IL4 stimulated B cells (CD40-B) and Plasmablast generated upon CD40+IL4 stimulation (CD40-PB). Inset: zoomed view of *Rel* expression in SplPB, SplPC and BMPC. The data were analyzed using deposited RNA_Seq data (GEO: GSE60927; Shi et al., 2015). The number of replicates in the bar graph depends on available dataset. **F)** Gating strategy and flow cytometry plot showing purity of fluorescence-activated-cell-sorted GC B cells as determined by B220$^{+}$FAS$^{+}$CD38$^{-}$. Cell percentage of GC B cells in the B220$^{+}$ lymph node cells (1.82%) and purity of GC B cells (99%). **G)** Gating strategy and flow cytometry plot showing purity of fluorescence-activated-cell-sorted ASCs as determined by B220$^{low}$CD138$^{+}$. Cell percentage of LN-ASCs in B220$^{high,low}$ lymph node cells (8.78%) and purity of ASCs (95.8%). **H)** Bar graph of mRNA expression by pPCR of *Blimp1*, *Bach2* and *IRF4* quantified in B cells, ABCs and LPS-PBs. Standard deviation of three replicates is indicated. **I)** Bar graph of mRNA expression of *Blimp1*, *Bach2* and *IRF4* quantified in naïve B cells, GC B cells and LN-ASCs. Ubiquitin C was used as housekeeping gene to quantitate mRNA expression. The standard deviation of three replicates is indicated. **J)** Contour plot of cRel and Blimp1 expression in intestinal B cell and intestinal ASCs (I-ASC). Black and green contour indicate B cell and I-ASC respectively. **K)** Bar graph of Mean Fluorescence Intensity (MFI) of cRel and Blimp1 in B cells and I-ASCs. **L)** Bar graph *Rel* mRNA expression quantified in unstimulated BCL1 (control) and stimulated BCL1 cells (IL-2+5 24h). **M)** Representative immunoblot of cRel, Blimp1, Bach2 and actin in unstimulated (control) and stimulated (IL-2+5 24h) in both BCL1 and BCL1-cRel cells. **N)** Bar graph of the percentage of actively cycling cells (S/G2 phase) in unstimulated (control, blank) and stimulated (IL-2+5 24h, shaded) in both BCL1 cells (gray) and

BCL1-cRel cells (blue). **O)** Immunoblot of Bach2 and actin in BCL1-cRel cells and *Bach2⁻ᐟ⁻* BCL1-cRel cells. The mean and standard deviation of three replicates is shown.   *p < 0.05, **p < 0.01, ***p < 0.001 and not significant (ns) Unpaired Students t-test).
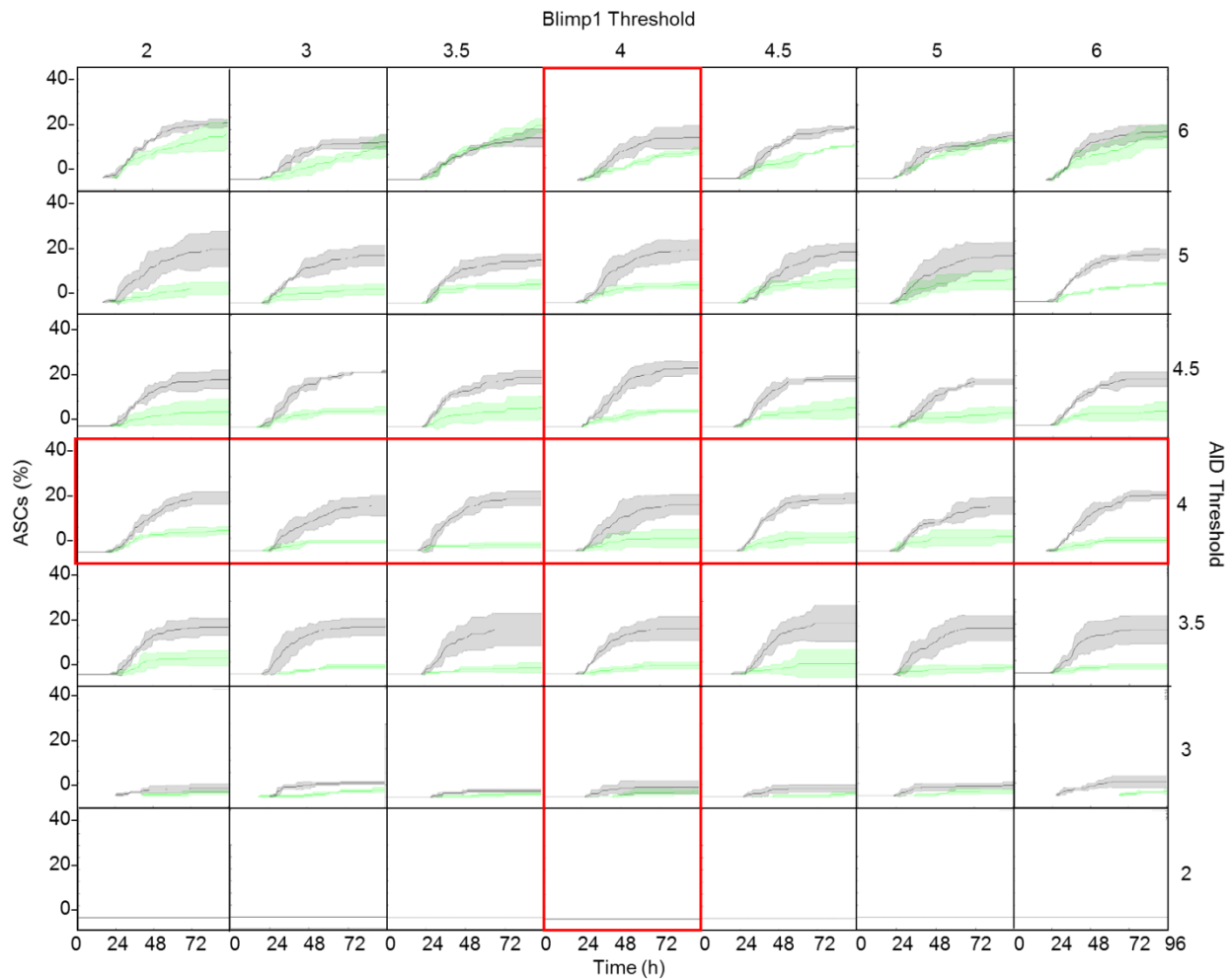


**Figure S3 (Related to Figure 3): ASC inhibition by cRel is robust to chosen threshold parameters.** Percentage ASC production over time (h) in simulations with the model v1 (without cRel-Blimp1 inhibition, green) and v2 (with cRel-Blimp1 inhibition, grey) using the indicated thresholds of Blimp1 and AID to determine cell fate. The solid line indicates the mean and shaded region indicates the standard deviation of 3 simulations, each containing 125 founder cells. The red box indicates the threshold used in Figure 3B.

A

BCL1    *Blimp1^{-/-}* BCL1

Blimp1

1       0.07

Actin

B

Experiment

*Rel*

Fold Change

8

4

0

WT    *Blimp1^{+/-}*    *Blimp1^{-/-}*

C

3 %   CATCTGAAAGCC**TGG**CTTCA

32 %  CATCTGAAA**A**GCCTGGCTTCA

15 %  CATCTGAA-GCCTGGCTTCA

4 %   CATCTGAAA**AA**GCCTGGCTTCA

3 %   CATCTGA--GCCTGGCTTCA

D

*Rel*

☐ H3K9ac
■ IgG

% Input (Chip-qPCR)

2

1

0

***

B cell    ABC    LPS-PB

E

*Rela*

2

1

0

ns

B cell    ABC    LPS-PB

F

ABC

200

0

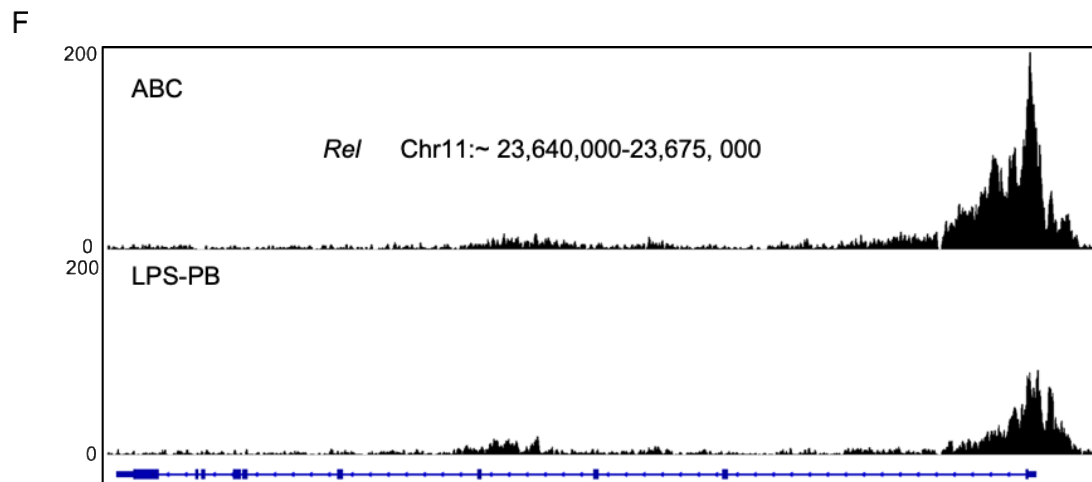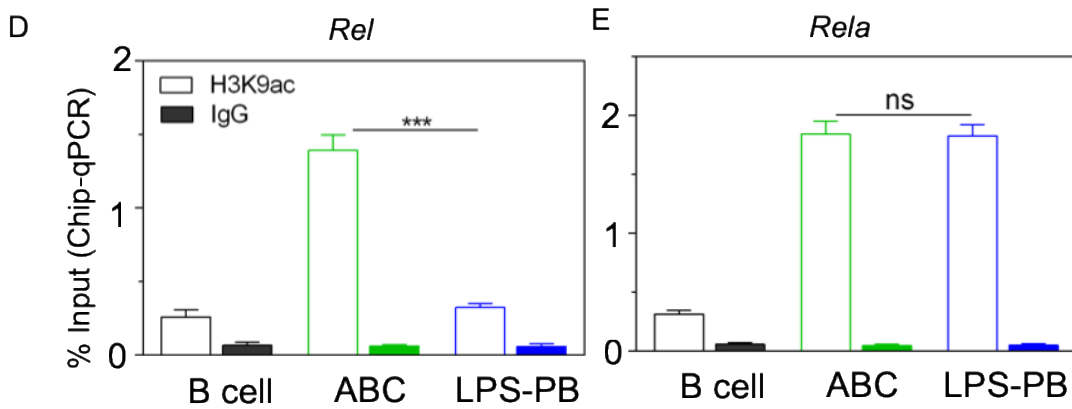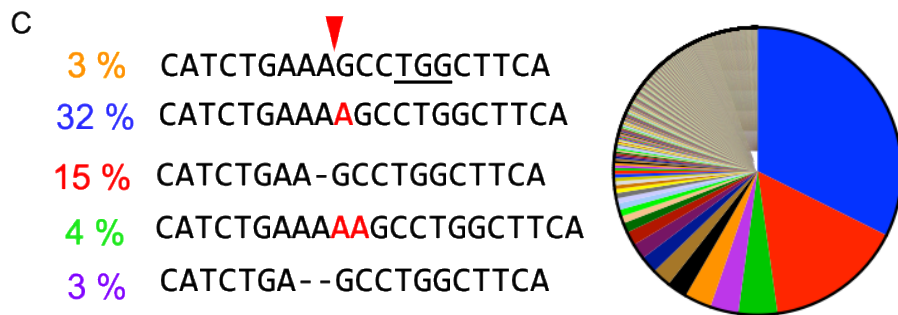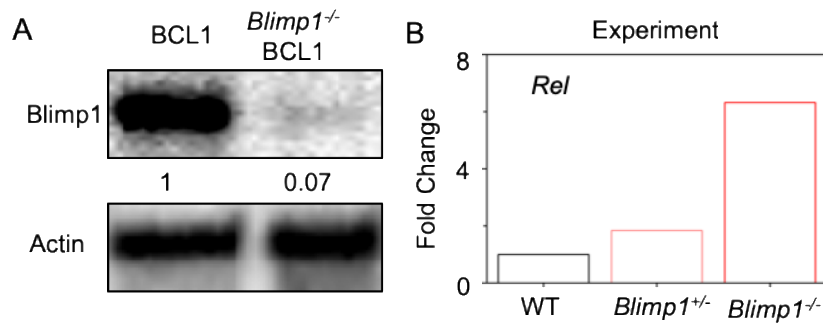*Rel*   Chr11:~ 23,640,000-23,675, 000

LPS-PB

200

0

**Figure S4 (Related to Figure 4): Analysis of Cas9/CRISPR-generated mutants and H3K9ac abundance on *Rel* locus. A)** Immunoblot of Blimp1 and actin in BCL1 cells and *Blimp1*^{-/-} BCL1 cells. The quantification of Blimp1 relative to BCL1 cells is indicated below. **B)** Bar graph showing fold change of *Rel* expression in wild-type, *Blimp1*^{+/-}, *Blimp1*^{-/-} B-cells analyzed from deposited RNA-seq data (GEO: GSE70981; Tellier et al., 2016) and reported relative to wild-type B-cells. **C)** Analysis of the targeted locus in *Rel*[BS-mut] BCL1 cells. Percentages of the total pool of sequences obtained from a population of cells (left). Cas9 binding sites (TGG) are indicated by an underline and target sites are indicated by a red arrow. Pie chart of the frequency of each sequence within the pool (right). **D)** and **E)** ChIP-qPCR for H3K9ac and IgG (isotype control) at the *Rel* (**D**) and *Rela* locus (**E**) in B cells (black), ABCs (green) and LPS-PBs (blue). LPS-PBs and ABCs were generated by stimulating B cells with LPS for 72 h. H3K9ac and IgG (isotype control) enrichment was calculated with respect to Input. The mean and standard deviation of three replicates is shown. $*p < 0.05$, $**p < 0.01$, $***p < 0.001$ and not significant (ns) (Unpaired Students t-test). **F)** Analysis of H3K9ac ChIP-seq data of ABCs and LPS-PBs on the *Rel* locus. The data were processed from a deposited data (GEO: GSE71698; Minnich et al., 2016).

**A**

Blimp1 Threshold

**B**

**C**

**D**

**E**

**F**

Blimp1    Bach2    IRF4

**Figure S5 (Related to Figure 5): ASC phenotype in *Rel*^{-/-} B cell. A)** Time course plot of percentage (%) increase of ASCs in cRel-deficient (cRel^{-/-}) B cells compared to wild type (WT) controls as predicted by mathematical modeling using the NFκB-extended ASC differentiation model v2 and the indicated thresholds of Blimp1 and AID to determine cell fate.  The solid line indicates the mean and shaded region indicates the standard deviation of 3 replicates with 125 initial cells. The red box indicates the threshold used in Figure 5A. **B)** Flow cytometry plot of LPS-PBs cell percentage over time in wild type (WT) and *Rel*^{-/-} B cells tracked at indicated timepoints. The LPS-PBs (B220^{low}, CD138^{+}) cell percentage is indicated in each plot. **C)** Bar graph of the percentage loss of ABCs and LPS-PBs in *Rel*^{-/-} cells over WT cells at 48 h and 72 h, calculated as: $([WT\ ASC\ count] - [Rel -/- ASC\ count])/[WT\ ASC\ count])$ and $([WT\ ABC\ count] - [Rel -/- ABC\ count])/[WT\ ABC\ count])$. Percentage cell loss is indicated in each graph. **D)** Representative flow cytometry plot of the percentage of apoptotic cells (Annexin V^{+}PI^{-} cell) in wild type ABCs and LPS-PBs at 72 h. The percentage of apoptotic cells indicated in each plot. **E)** Bar graph showing the percentage of apoptotic cells within WT-ABCs, cRel^{-/-}-ABCs, WT- LPS-PBs and *Rel*^{-/-}-LPS-PBs at 72 h. The fold change of apoptotic cells between WT (black) and *Rel*^{-/-} (red) is indicated.  **F)** Bar graphs of Blimp1, Bach2, and IRF4 mRNA expression quantified in WT (black) and *Rel*^{-/-} (red) B cells at 0 h, 24 h, 36 h, 48 h, 60 h and 72 h following stimulation with LPS. The mean and standard deviation of three replicates is indicated. *p < 0.05, **p < 0.01, ***p < 0.001 and not significant (ns) (Unpaired Students t-test).
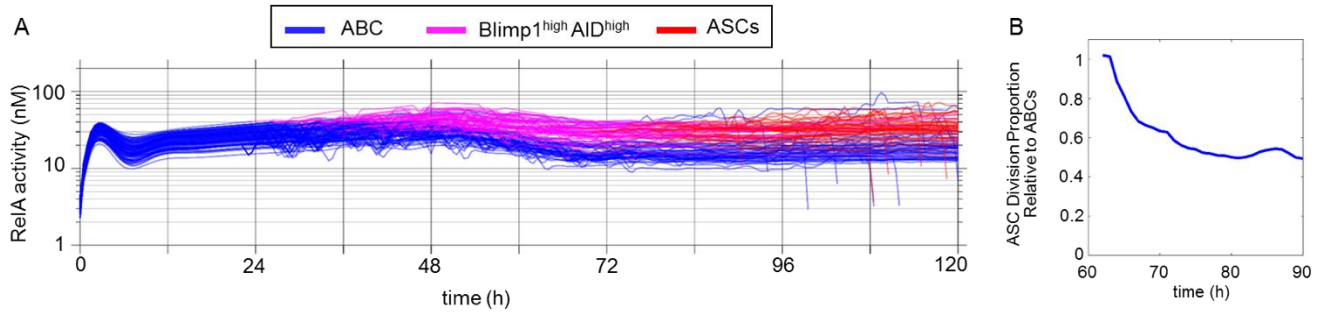
**Figure S6 (Related to Figure 6): Prediction of ASC generation kinetics with simulation of RelA and proportion of dividing ASC. A)** Line plots of average RelA activity (nuclear RelA:p50 concentration) within 200 simulated lineages. Each line represents the average concentration of progeny from a single founder cell. ASC generating lineages are indicated as ABCs (blue) transition to Blimp1$^{high}$AID$^{high}$ (pink) and ASCs (red). X-axis indicates time (h) and Y-axis indicates simulated nuclear RelA:p50 heterodimer concentrations (nM). **B)** Line graph of the proportion of cells that will divide at least once among ASCs relative to the proportion of cells dividing among ABCs over time (h). A value of 1 indicates the same number of dividing cells among ABCs and ASCs, while <1 indicates ASCs are less likely to divide than ABCs.
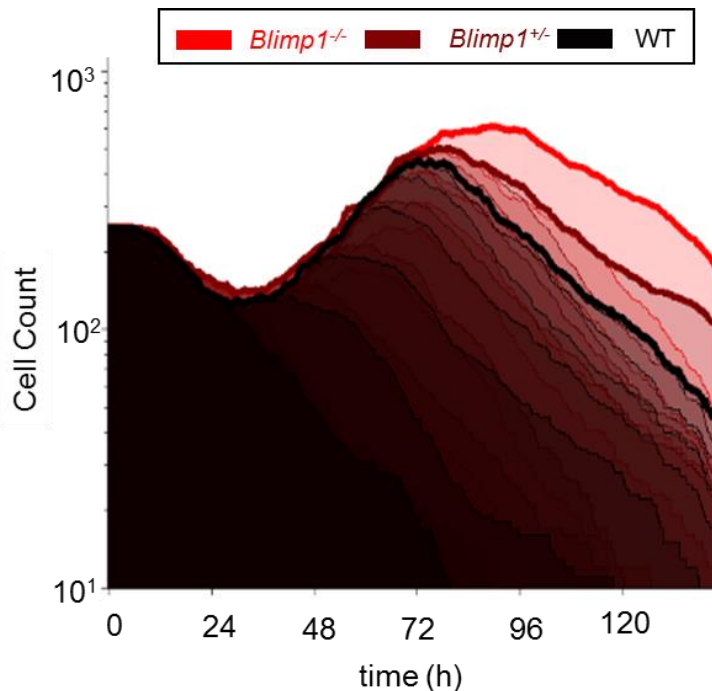


**Figure S7 (Related to Figure 7): B cell population dynamics upon perturbation of *Blimp1*.** Stacked area plot of B cell counts in WT (black), *Blimp1$^{+/-}$* (maroon), *Blimp1$^{-/-}$* (red) simulations over time (h). Each simulation contained 125 founder cells.

**Table S1 (Related to Figure 1): Regulatory network connections in the model**

| Regulatory Connection | | | Source |
|---|---|---|---|
| IRF4 | Promotes | Blimp1 | Sciammas *et al.* 2011 |
| Blimp-1 | Promotes | IRF4 | Sciammas *et al.* 2011 |
| Blimp-1 | Inhibits | Pax5 | Sciammas *et al.* 2011 |
| IRF4 | Inhibits | Bach2 | Sciammas *et al.* 2011 |
| IRF4 | Promotes | AID | Sciammas *et al.* 2011 |
| Blimp-1 | Inhibits | Bach2 | Sciammas *et al.* 2011 |
| Bach2 | Inhibits | Blimp1 | Sciammas *et al.* 2011 |
| Pax5 | Promotes | Bach2 | Sciammas *et al.* 2011 |
| Pax5 | Promotes | AID | Sciammas *et al.* 2011 |
| RelA | Promotes | IRF4 | Siato *et al.* 2007 |
| cRel | Promotes | IRF4 | Grumont *et al.* 2000 |
| cRel | Promotes | Bach2 | Hunter *et al.* 2016 |
| RelA | Promotes | Blimp-1 | Morgan *et al.* 2009 |
| cRel | Promotes | AID | Park *et al.* 2009 |
| RelA | Promotes | AID | Park et al. 2009 |

**Table S2 (Related to Figures 1, 3 and 6): Parameter values in the model**

| | | Param | Value | Justification |
|---|---|---|---|---|
| IRF-4 | Act | $k_{aI}$ | 7.5 | Sciammas *et al.* 2011 |
| | | $n_{aI}$ | 2 | |
| | | $K_{aI}$ | 1 | |
| | Deg | $d_I$ | 1 | |
| BLIMP-1 | Act | $k_{aB}$ | 7.5 | Sciammas *et al.* 2011 |
| | | $n_{aB}$ | 2 | |
| | | $K_{aB}$ | 3 | Increased from published value of 1 to ensure sensitivity to RelA and IRF4 |
| | Rep | $K_{rB}$ | 1 | Sciammas *et al.* 2011 |
| | | $n_{rB}$ | 2 | |
| | Deg | $d_B$ | 1 | |
| Pax5 | Basal | $e_P$ | 2 | Sciammas *et al.* 2011 |

| | | | | |
|---|---|---|---|---|
| | Rep | $K_{rP}$ | 1 | |
| | | $n_{rP}$ | 2 | |
| | Deg | $d_P$ | 1 | |
| Bach2 | Act | $k_{aH}$ | 7.5 | Sciammas *et al.* 2011 |
| | | $n_{aH}$ | 1 | |
| | | $K_{aH}$ | 1 | |
| | Rep | $K_{rH}$ | 1 | |
| | | $n_{rH}$ | 2 | |
| | Deg | $d_H$ | 1 | |
| AID | Act | $k_{aA}$ | 0.375 | Half published value of 0.75 to allow for activation by RelA and cRel. |
| | | $n_{aA}$ | 1 | Sciammas *et al.* 2011 |
| | | $K_{aA}$ | 1 | |
| | Deg | $d_A$ | 0.1 | |
| cRel | Basal | $\bar{e}_C$ | 1 | Chosen to replicated modeling strategy of Sciammas *et al.* 2011 |
| | Rep | $K_{rC}$ | 1 | |
| | | $n_{rC}$ | 2 | |
| | Deg | $d_C$ | 0.1 | |
| RelA | Basal | $e_R$ | 1 | Chosen to replicated modeling strategy of Sciammas *et al.* 2011 |
| | Act | $k_{aR}$ | 0.75 | |
| | | $K_{aR}$ | 1 | |
| | | $n_{aR}$ | 2 | |
| | Deg | $d_R$ | 0.1 | |

**Table S3 (Related to Figures 2, 4 and 5): Sequences of primers**

| mRNA qPCR primers | |
|---|---|
| Rela | GCAGTATCCATAGCTTCCAG |
| | TGCTCCTCTATAGGAACGTG |
| Rel | TTGCAGAGATGGATACTATGAAGC |
| | CACCGAATACCCAAATTTTGAA |
| Blimp1 | GGCTCCACTACCCTTATCCTG |
| | TTTGGGTTGCTTTCCGTTT |
| Bach2 | CAGTGAGTCGTGTCCTGTGC |
| | TTCCTGGGAAGGTCTGTGAT |
| IRF4 | ATTCCAGGTGACTCTGTGCT |
| | TGGAGTGGTAACGTGTTCAG |
| Ubiqutin C | GCCCAGTGTTACCACCAAGA |
| | CCCATCACACCCAAGAACA |
| ChIP qPCR primers | |
| Rel | TGAAACACCCCAGTTTCCTT |
| | CAGGACGCTGACCCTTATCT |
| Rela | TCTGGCGAATGGCTTTACTT |
| | CAGAAAGGGGCGGAAGAC |

**Data S1 (Related to Figures 1, 3 and 6): Equations of the Mathematical Model**

$$\frac{d[BLIMP]}{dt} =$$

$$\left(\frac{k_{aB} \cdot [IRF]^{n_{aB}}}{K_{aB}^{n_{aB}} + [IRF]^{n_{aB}}} + \frac{k_{aB} \cdot [RelA]^{n_{aB}}}{K_{aB}^{n_{aB}} + [RelA]^{n_{aB}}}\right) \cdot \left(\frac{K_{rB}^{n_{rB}}}{K_{rB}^{n_{rB}} + [Bach2]^{n_{rB}}}\right) - d_B \cdot [BLIMP]$$

$$\frac{d[Pax]}{dt} =$$

$$e_P \cdot \left(\frac{K_{rP}^{n_{rP}}}{K_{rP}^{n_{rP}} + [BLIMP]^{n_{rP}}}\right) - d_P \cdot [Pax]$$

$$\frac{d[IRF]}{dt} =$$

$$\left(e_P + \frac{\frac{k_{aI}}{3} \cdot [BLIMP]^{n_{aI}}}{K_{aI}^{n_{aI}} + [BLIMP]^{n_{aI}}} + \frac{\frac{k_{aI}}{40} \cdot [cRel]^{n_{aI}}}{K_{aI}^{n_{aI}} + [cRel]^{n_{aI}}} + \frac{\frac{k_{aI}}{40} \cdot [RelA]^{n_{aI}}}{K_{aI}^{n_{aI}} + [RelA]^{n_{aI}}}\right) - d_I \cdot [IRF]$$

$$\frac{d[Bach2]}{dt} =$$

$$\left(\frac{k_{aH} \cdot [Pax]^{n_{aH}}}{K_{aH}^{n_{aH}} + [Pax]^{n_{aH}}} + \frac{k_{aH} \cdot [cRel]^{n_{aH}}}{K_{aH}^{n_{aH}} + [cRel]^{n_{aH}}}\right) \cdot \left(\frac{K_{rH}^{n_{rH}}}{K_{rH}^{n_{rH}} + [BLIMP]^{n_{rH}} + [IRF]^{n_{rH}}}\right) - d_H \cdot [Bach2]$$

$$\frac{d[AID]}{dt} =$$

$$\left(\frac{k_{aA} \cdot ([IRF] \cdot [Pax]^2)^{n_{aA}}}{K_{aA}^{n_{aA}} + ([IRF] \cdot [Pax]^2)^{n_{aA}}} + \frac{k_{aA} \cdot [cRel]^{n_{aA}}}{K_{aA}^{n_{aA}} + [cRel]^{n_{aA}}} + \frac{k_{aA} \cdot [RelA]^{n_{aA}}}{K_{aA}^{n_{aA}} + [RelA]^{n_{aA}}}\right) - d_A \cdot [AID]$$

$$\frac{d[cRel]}{dt} = e_C - d_C \cdot [cRel]$$

$$\frac{d[RelA]}{dt} = e_R - d_R \cdot [RelA]$$

## Data S2 (Related to Figure S4C): Code of CRISPR mutation analysis

```
01. #!/usr/bin/env python3
02. # -*- coding: utf-8 -*-
03. """
```

```python
Created on Mon Oct 29 16:28:34 2018
@author: Yi Liu @UCLA
"""
### fastx pre-processing bash scripts
# ./fastq_quality_filter -q 35 -p 95 -i BK01-KR_R1_001.fastq -o trimmed_35_95.fastq -v -Q33
# bin/fastx_quality_stats -i trimmed_35_95.fastq -Q33

# import pandas module for DataFrame tools
import pandas as pd

# read fastQ for sequences only forward ACTT, same results with the other strand
myls = []
with open('trimmed_35_95.fastq', 'r') as fh:
    for i, line in enumerate(fh):
        if i%4==1:
            if str.startswith(line, 'ACTT'):
                myls.append(line)

df = pd.DataFrame(myls)

# count unique sequences
dfCounts = df[0].value_counts().to_frame('counts').reset_index()

# truncate to site
dfCounts['site'] = dfCounts['index'].apply(lambda x: x[60:])
dfCounts['site_bothend'] = dfCounts['site'].apply(lambda x: x[:20])

# counts minor sequences
dfCounts['counts'].iloc[30:].sum()
dfCounts['counts'].iloc[10:].sum()
dfCounts['counts'].sum()

# export analysis results
dfCounts.to_csv('data_35_95.csv')

# plot results
dfCounts['counts'].plot.pie()

## check wild type and mutant sequence

# check first sequence for programming
dfCounts['site_bothend'].isin(['CATCTGAAAAGCCTGGCTTC'])

# find wild type sequence in results
dfCounts['site_bothend'].isin(['CATCTGAAAGCCTGGCTTCA'])

# verify if found wild type sequence to known wild type sequence from Pubmed
fromNGS = 'ACTTAAAGCCTTTTTGTGCTTCTAATCAGAACATGAGTTAAATTTACAAATTTACTAGAGCATCTGAAAGCCTGGCTTCATTTAAATGGGTAAAGAGAAAGTTGAAATATTTTAAACTACACTTGTTTTCTCATGAAAACCACAGACAAACTGAAATCAAGTGTCATGTGAAACACCCCAGTTTCCTTTACAGCAGGAGTT'
fromPub = 'ACTTAAAGCCTTTTTGTGCTTCTAATCAGAACATGAGTTAAATTTACAAATTTACTAGAGCATCTGAAAGCCTGGCTTCATTTAAATGGGTAAAGAGAAAGTTGAAATATTTTAAACTACACTTGTTTTCTCATGAAAACCACAGACAAACTGAAATCAAGTGTCATGTGAAACACCCCAGTTTCCTTTACAGCAGGAGTT'
fromNGS == fromPub
```